JACS
JOURNAL OF THE AMERICAN CHEMICAL SOCIETY

Article

pubs.acs.org/JACS

Mechanistic Insights on the *ortho*-Hydroxylation of Aromatic Compounds by Non-heme Iron Complex: A Computational Case Study on the Comparative Oxidative Ability of Ferric-Hydroperoxo and High-Valent Fe^{IV}=O and Fe^{V}=O Intermediates

Azaj Ansari, Abhishek Kaushik, and Gopalan Rajaraman*

Department of Chemistry, Indian Institute of Technology Bombay, Mumbai 400076, India

Supporting Information

ABSTRACT: *ortho*-Hydroxylation of aromatic compounds by non-heme Fe complexes has been extensively studied in recent years by several research groups. The nature of the proposed oxidant varies from Fe^{III}–OOH to high-valent Fe^{IV}=O and Fe^{V}=O species, and no definitive consensus has emerged. In this comprehensive study, we have investigated the *ortho*-hydroxylation of aromatic compounds by an iron complex using hybrid density functional theory incorporating dispersion effects. Three different oxidants, Fe^{III}–OOH, Fe^{IV}=O, and Fe^{V}=O, and two different pathways, H-abstraction and electrophilic attack, have been considered to test the oxidative ability of different oxidants and to underpin the exact mechanism of this regiospecific reaction. By mapping the potential energy surface of each oxidant, our calculations categorize Fe^{III}–OOH as a sluggish oxidant, as both proximal and distal oxygen atoms of this species have prohibitively high barriers to carry out the aromatic hydroxylation. This is in agreement to the experimental observation where Fe^{III}–OOH is found not to directly attack the aromatic ring. A novel mechanism for the explicit generation of non-heme Fe^{IV}=O and Fe^{V}=O from isomeric forms of Fe^{III}–OOH has been proposed where the O···O bond is found to cleave via homolytic (Fe^{IV}=O) or heterolytic (Fe^{V}=O) fashion exclusively. Apart from having favorable formation energies, the Fe^{V}=O species also has a lower barrier height compared to the corresponding Fe^{IV}=O species for the aromatic *ortho*-hydroxylation reaction. The transient Fe^{V}=O prefers electrophilic attack on the benzene ring rather than the usual aromatic C–H activation step. A large thermodynamic drive for the formation of a radical intermediate is encountered in the mechanistic scene, and this intermediate substantially diminishes the energy barrier required for C–H activation by the Fe^{V}=O species. Further spin density distribution and the frontier orbitals of the computed species suggest that the Fe^{IV}=O species has a substantial barrier height for this reaction, as the substrate is coordinated to the metal atoms. This coordination restricts the C–H activation step by Fe^{IV}=O species to proceed via the π-type pathway, and thus the usual energy lowering due to the low-lying quintet state is not observed here.

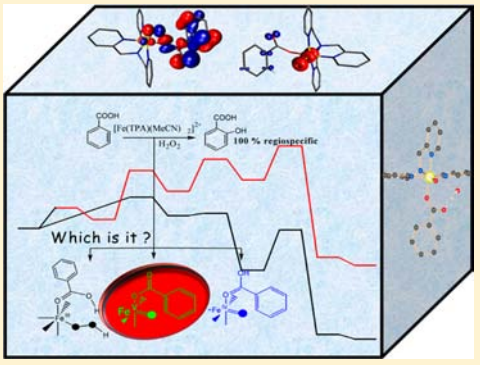

INTRODUCTION

Metal-catalyzed selective hydroxylation of aromatic compounds has gained attention in recent years, as this reaction forms an important precursor in the pharmaceutical industry.[1] Iron-catalyzed hydroxylation has been reported with Fenton's reagent, but these reactions are often nonselective due to the generation of hydroxyl radicals.[2] On the other hand, many metal complexes reported in recent years catalyze this reaction efficiently with very high selectivity.[3] Among others, reactions catalyzed by non-heme iron oxidants have been the subjects of extensive study since the development of regio- and stereoselective catalytic oxidation of organic substrates. These reactions are particularly attractive because they are based on cheap, nontoxic reactants (usually O_2 or H_2O_2 as oxidants and Fe, Cu, or Mn complexes as catalysts). Considerable progress has been made in this area, which includes crystallization and characterizations of several high-valent iron intermediates[3g,4] as well as discovery of synthetically useful, regioselective epoxidations and hydroxylations catalyzed by biomimetic iron complexes.[5] Much of this chemistry is biomimetic, as many enzymes (non-heme iron active site in pterin-dependent aromatic amino acid hydroxylases[6] and methane and toluene monooxygenases,[7] for example) in nature possess mono-/dinuclear non-heme iron sites to effect the catalysis. The key to understand the catalytic mechanism of these enzymes is the development of synthetic model compounds that mimic their catalytic activity and a thorough investigation of their structural, electronic, and mechanistic pathways. In this regard, the mechanism of iron-promoted *ortho*-hydroxylation reaction remains elusive and is the topic of current research in the bioinorganic chemistry community.

High-valent iron–oxo species are reported to be important intermediates in reactions with mononuclear non-heme iron

Received: July 19, 2012
Published: February 1, 2013

   dx.doi.org/10.1021/ja307077f | *J. Am. Chem. Soc.* 2013, 135, 4235–4249

Scheme 1. Mechanism of *ortho*-Hydroxylation of Aromatic Compounds Mediated by Iron Complexes

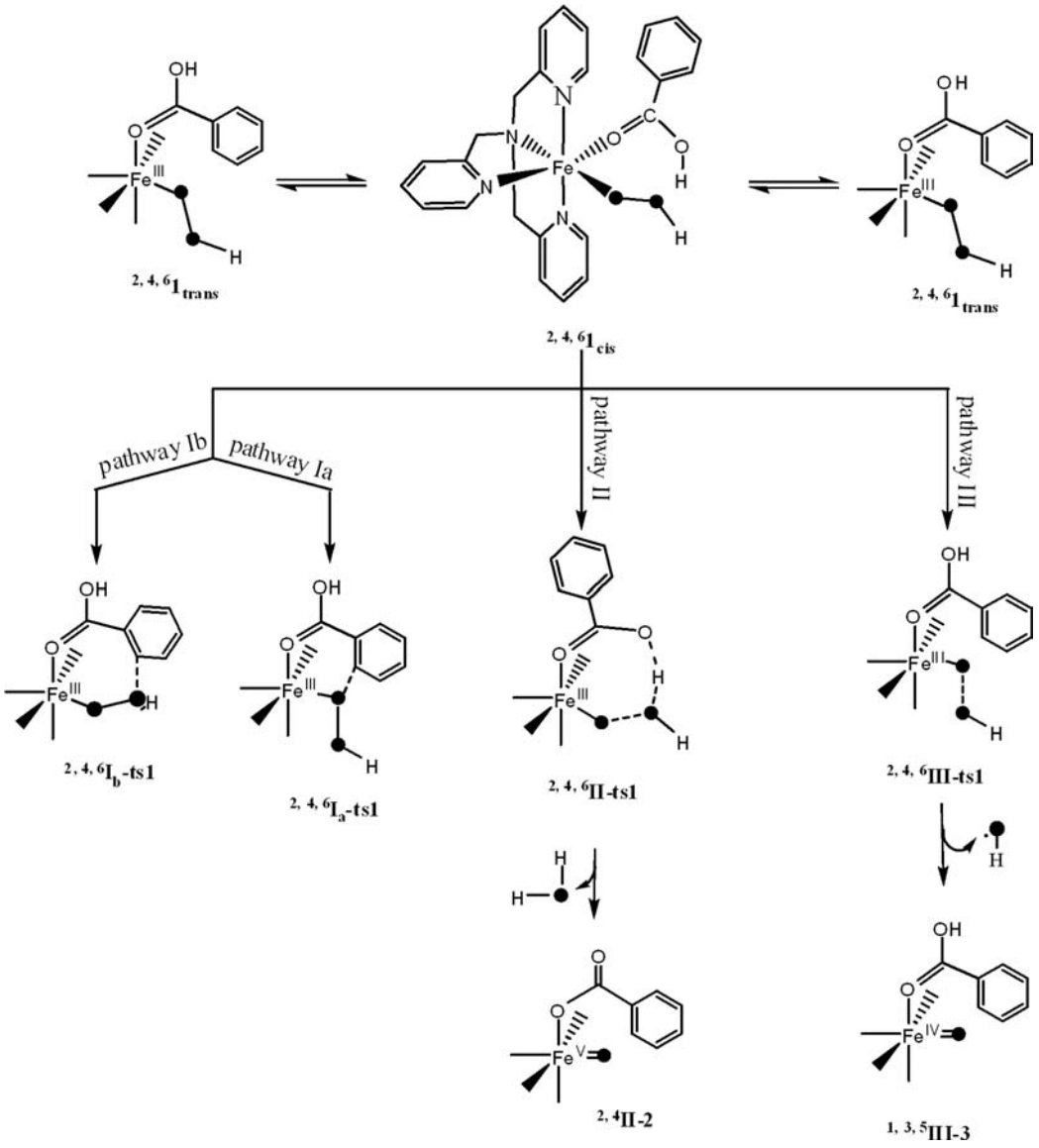

enzyme as well as heme iron enzymes.[8] The proposed mechanism features an electrophilic high-valence iron−oxo group as oxidant, and this is supported by the experimental and theoretical work.[9] In the past decade, Fe^{IV}=O species have aroused much interest in the scientific community due to their catalytic properties, ranging from alkane oxidation to aromatic hydroxylation.[10] The Fe^{IV}=O compounds are characterized as intermediates in many catalytic reactions with iron-containing enzymes.[5,11] One of the most widely studied examples is cytochrome P450, which catalyzes a very difficult reaction: oxidation of an alkyl group to an alcohol.[12] The P450 is a well-characterized heme enzyme known to catalyze a variety of reactions, such as oxidation, reduction, isomerization, and dehydration.[12c,d] Our understanding of enzymatic reactions has been greatly improved by studying the spectroscopic and chemical properties of heme and non-heme Fe^{IV}=O complexes.[4a,13,14] Que et al., in their seminal work, reported the generation of a mononuclear non-heme complex with a terminal Fe^{IV}=O unit and described its spectroscopic properties and high-resolution crystal structure.[4a,c,15] Various spectroscopic techniques, such as electronic, magnetic circular dichroism, Raman, electron paramagnetic resonance (EPR), and Mossbauer spectroscopy, are commonly used to characterize ferryl−oxo complexes.[13a,14a,15,16] Recently, Nam et al. illustrated that EPR spectroscopy can be used to detect high-spin ferryloxo species.[17] On the other hand, quantum chemical studies are also widely used to underpin the chemical bonding and reactivity of heme and non-heme Fe^{IV}=O complexes.[14b,d,e,15]

Besides the Fe^{IV}=O intermediates, the Fe^{V}=O species are also considered to be highly reactive intermediates in a large number of enzymatic oxidations, as well as certain Fe/H_2O_2 systems.[18] The first convincing chemical and spectroscopic evidence for the presence of the Fe^{V}=O species was reported by Que et al. with a tetraamido macrocyclic ligand,[19] and its detection in the C−H activation process was due to the work of Costas et al. using variable-temperature mass spectrometry.[18,19a,20] Using a bunch of spectroscopic techniques, Que et al. have recently detected the Fe^{V}=O species with the cyclam ligand.[21] A specific study which is relevant to our work is the detection of Fe^{V}=O species containing aminopyridine ligand systems such as tris(2-pyridylmethyl)amine (TPA) and *N,N′*-

dx.doi.org/10.1021/ja307077f | J. Am. Chem. Soc. 2013, 135, 4235−4249

dimethyl-*N*,*N*′-bis(2-pyridylmethyl)ethane-1,2-diamine (BPMEN) using EPR spectroscopy.[19b]

Recently, iron-promoted selective *ortho*-hydroxylation of benzoic acid in the presence of H_2O_2 has been reported with various types of aminopyridine ligand backbones.[3g,h,9g] Particularly the biomimetic catalysts $[Fe^{II}(TPA)(CH_3CN)_2]^{2+}$ (**1**) and $[Fe^{II}(BPMEN)(CH_3CN)_2]^{2+}$ are of significant importance, as numerous experimental studies have been undertaken on them. In our study on the subject, we use complex **1**, on which extensive spectroscopic and kinetic data have been accumulated, to probe the mechanism of *ortho*-hydroxylation.[3g,h,15b,22] Complex **1** catalyzes the *ortho*-hydroxylation of various benzoic acid derivatives, leading to the formation of salicylic acid. Some substituted benzoic acid derivatives, on the other hand, yield *ipso*-hydroxylated product. The regiospecificity of these reactions indicates that a metal-based oxidant is likely to trigger the catalytic reaction. This is supported by ^{18}O labeling experiments which indicate that one of the oxygens of the labeled H_2O_2 is incorporated in the product formation. The Fe^{III}−OOH species is suggested as an obvious starting point, as this species has been spectroscopically detected during the course of the reaction[10t,23] and has been hypothesized as one of the potential oxidants which could directly attack the aromatic ring. On the other hand, the O···O bond of the Fe^{III}−OOH species could cleave homolytically or heterolytically, leading to a transient Fe^{IV}=O or Fe^{V}=O species, respectively, both of which are also potential oxidants in this chemistry. In the case of homolytic cleavage, the hydroxyl radicals are expected and may provide rather nonselective, scrambled products. However, there are cases where generation of a caged hydroxyl radical along with formation of Fe^{IV}=O species have been encountered.[24]

Although the experimental studies indicate that the unobserved Fe^{V}=O[3g,h] species is the likely oxidant in this reaction, an aggressive oxidative nature of Fe^{IV}=O complexes has been reported on various occasions,[25] and formation of Fe^{IV}=O even in the presence of acetic acid[26] raises ambiguity as to why this particular reaction prefers Fe^{V}=O rather than the Fe^{IV}=O oxidant. There are a few instances where the catalytic ability of Fe^{III}−OOH itself attacking the substrate has been explicitly probed. Nam et al., testing it for the oxidation of olefins and sulfides, suggested that the Fe^{III}−OOH is a sluggish oxidant.[27] However, studies by Solomon et al. fully support Fe^{III}−OOH as the active oxidant which attacks DNA directly in activated bleomycin (ABLM).[28] Considering the fact that O···O cleavage is required to generate transient Fe^{IV}=O or Fe^{V}=O species (see Scheme 1), and this step has been estimated to have relatively high barrier,[29] while the direct attack of Fe^{III}−OOH escapes this route motivates us to also consider Fe^{III}−OOH as a potential oxidant in this reaction.

Taking into account all the above points, here we report extensive computational studies on the mechanism of *ortho*-hydroxylation of benzoic acid using complex **1** with H_2O_2. In our mechanistic study on the topic, we propose various possible reaction pathways for *ortho*-hydroxylation using Fe^{III}−OOH. Three questions are addressed and discussed in this study: (1) Which types of high-valent intermediates are of importance in this catalytic transformation? (2) What are the energetics/electronic preferences for a particular oxidant to favor a given reaction? (3) What are the mechanistic pathways (see Scheme 1 for a general mechanistic pathway based on experimental input and previous theoretical studies)[3g,30] by which these high-valent oxidants effect the transformation very selectively?

COMPUTATIONAL DETAILS

All calculations were performed using the Gaussian 09 suite of programs.[31] Geometry optimizations were carried out using the B3LYP-D3 functional.[32] The B3LYP-D3 functional incorporating the dispersion proposed by Grimme et al.[32] is widely employed and is the state-of-the-art functional used to understand the mechanism of metal-mediated catalytic reactions. Calculations were also performed using several other functionals, including conventional B3LYP, which is routinely used in Fe catalysis.[33,34] Structure optimizations were carried out using Gordon's[35] wB97XD, Grimme's[32b] B97D, and Truhlar's M06-2X[36] functionals along with single-point energy calculations performed using TPSSh[37] and OLYP[38] together with MP2[39] methods. The ground states of Fe^{III}−OOH, Fe^{IV}=O, and Fe^{V}=O have been spectroscopically determined to be $S = 5/2$,[40] $S = 1$,[4a,14o,41] and $S = 1/2$,[19] respectively, for non-heme metal complexes possessing similar structural motifs (amine and pyridine donor atoms), and these three species were taken as probes to validate the behavior of different functionals. Among the tested functionals, B3LYP, B3LYP-D3, and wB97XD yield correct ground states for all the three species, and so we chose B3LYP-D3 energies to describe the mechanism. For the H-abstraction reaction of the non-heme model system, method assessment was performed with RCCSD(T),[42] and B3LYP and B3LYP-D along with TPSSh were found to predict spin-state energetics close to those found with the RCCSD(T) method. This assessment adds further confidence to our computed energetics. However, we note here that there are instances when B3LYP predicts incorrect ground states, particularly for systems that have small low-spin and high-spin gaps, such as spin-crossover complexes.[43] A detailed analysis of the different methods studied is given in the Supporting Information, along with computed potential energy surfaces (PESs) for all the tested methodologies (see Discussion, Tables S1−S5, and Figures S1−S26). The LACVP basis set, comprising the LanL2DZ Los Alamos effective core potential for Fe[44] and a 6-31G basis set for the other atoms[45] (B-I), was employed for geometry optimization, and the optimized geometries were then used to perform single-point energy calculations using a TZVP[46] basis set (B-II) on all atoms. The solvation energies were computed using the PCM solvation model, employing acetonitrile as the solvent. Frequency calculations were performed on the optimized structures at the B-I level to verify that they are minima on the PES and also to obtain free energy corrections. The quoted DFT energies are B3LYP-D3 solvation energies incorporating free energy (ΔG) correction at the B-I level computed at 298.15 K, unless otherwise mentioned. The energy landscapes computed using only electronic energy with solvation (neglecting ZPE, vibrational, and thermal corrections) and using free energies are given in Figures S27−S32 for comparison. Both types of profiles show similar trends in terms of predicting the rate-limiting step and thermodynamic stability of the intermediates and products, with some variations in the absolute values. The transition states were characterized by a single negative frequency corresponding to the reaction coordinate and verified by animating the frequency using visualization software such as Molden.[47] For selected transition states, intrinsic reaction coordinate (IRC) calculations were performed to verify that the transition state indeed connects with the corresponding minimum stationary points associated with the reactants and products. The fragment approach available in Gaussian 09 is employed to aid smooth convergence in cases of radical intermediates. For spin-coupled states, Noodlemann's[48a] broken-symmetry method is employed to obtain correct polarized spin states. The nature of all the spin-coupled states after convergence was verified by analyzing the computed spin densities and $\langle S^2 \rangle$ values. The mean energy crossing points (MECPs) between different spin surfaces were computed for selected cases using the ad hoc code developed by Harvey et al.[48b] Due to convergence issues with B3LYP-D3 geometry optimizations for the MECPs, single-point energies were computed using B3LYP-D3 on B3LYP-optimized geometries. Detailed structures and energetics of the MECPs are given in the Supporting Information. A common notation of $^{mult}A_{isomer/spin\text{-}state}$ is employed throughout, where A stands for the different pathway/species involved in the PES, the mult superscript

dx.doi.org/10.1021/ja307077f | J. Am. Chem. Soc. 2013, 135, 4235−4249

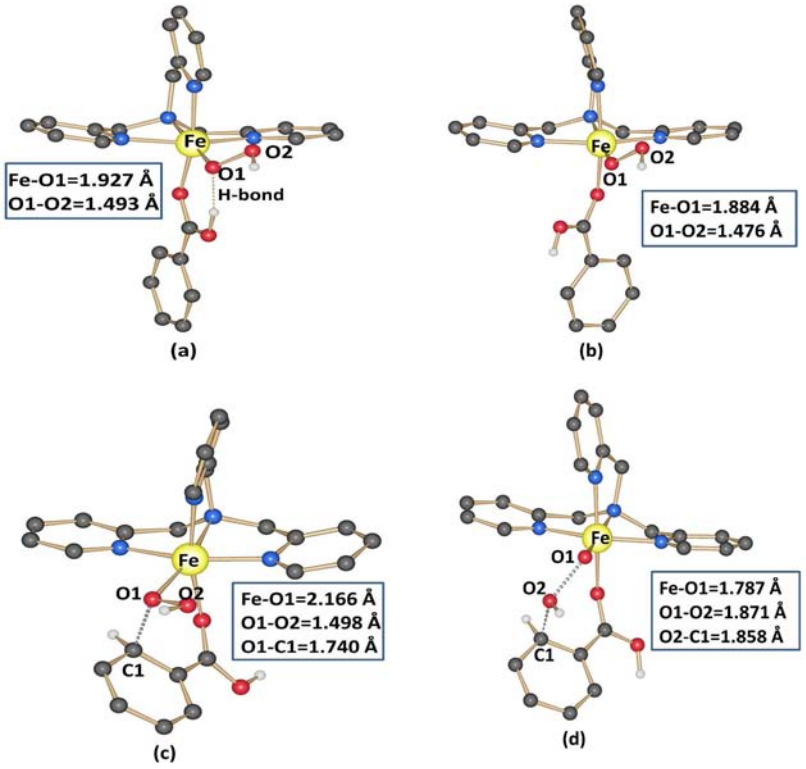

Figure 1. B3LYP-D3-optimized structure of the ground state with selected structural parameters: (a) $^{6}\mathbf{1}_{cis}$, (b) $^{6}\mathbf{1}_{trans}$ (c) $^{6}\mathbf{I}_{a}$-*ts1*, and (d) $^{6}\mathbf{I}_{b}$-*ts1*. Fe−O1 and O1−O2 (Å) distances for $^{4}\mathbf{1}_{cis}$ ($^{2}\mathbf{1}_{cis}$): 1.981 (1.855) and 1.506 (1.509), respectively. Fe−O1 and O1−O2 (Å) distances for $^{4}\mathbf{1}_{trans}$ ($^{2}\mathbf{1}_{trans}$): 1.814 (1.806) and 1.506 (1.508), respectively. Fe−O1, O1−O2, and O1−C1 distances (Å) for $^{4}\mathbf{I}_{a}$-*ts1* ($^{2}\mathbf{I}_{a}$-*ts1*): 2.095 (1.987), 1.503 (1.537), and 1.754 (1.787), respectively. Fe−O1, O1−O2, and O1−C1 distances (Å) for $^{2}\mathbf{I}_{b}$-*ts1*: 1.730, 1.977, and 1.787, respectively.

denotes the total multiplicity of the species, and the isomer/spin-state subscript denotes the possible *cis*/*trans* isomers or different spin configurations (high-spin, low-spin, etc.) on the Fe atom.

RESULTS

Based on inputs from experimental studies,[3g,h,22] Scheme 1 has been adopted to represent the mechanism of *ortho*-hydroxylation via three mechanistic pathways. Pathway I is based on the idea that the Fe^{III}−OOH species itself acts as an oxidizing agent, yielding *ortho*-hydroxylated product, while pathways II and III are based on the heterolytic or homolytic cleavage of the O···O bond of the Fe^{III}−OOH species, followed by the generation of the transient Fe^{V}=O or Fe^{IV}=O species which eventually trigger the catalytic reaction. The mechanisms of individual pathways I−III are discussed separately, and the different pathways are analyzed and compared in the Discussion section. The results are discussed in line with the available experimental data.[3g,h,22]

Pathway I. An obvious starting point with respect to the identification of a metal-based oxidant is an Fe^{III}−OOH intermediate, as this species has been fully characterized starting from the $[Fe^{II}(TPA)\ (CH_3CN)_2]^{2+}$ precursor.[41a,b] Initial checks were made to determine the lowest energy positional isomerism, where the −OOH group coordinating trans to the amine nitrogen is found to be the lowest in energy (by 8.8 kJ/mol; see Figure S33), and this agrees with the experimental findings.[3g] Within the lowest positional isomer, further isomerism is possible based on the orientation of the acidic (−COOH) group of the coordinated benzoic acid. The −OH group of the benzoic acid can be either *cis* to the Fe−OOH group or *trans* (see Scheme 1). In the *cis* position, the −OH group is expected to be in an H-bonding interaction with the proximal oxygen atom. For both $\mathbf{1}_{cis}$ and $\mathbf{1}_{trans}$ isomers, the high-spin sextet is found to be the ground state (see Figure 1). The optimized structural parameters and the spin-state energetics are consistent with previous theoretical reports.[49] Between these two isomers, $^{6}\mathbf{1}_{cis}$ is found to be stabilized by 19.9 kJ/mol compared to the corresponding *trans* isomer. There is a strong H-bonding interaction between the −COOH group of the benzoic acid and the proximal oxygen of the −OOH group, and this interaction stabilizes the *cis* isomer over the *trans* isomer. The H-bonding interaction also weakens the Fe−O and O···O bond lengths in the *cis* isomer compared to the *trans* isomer (see Figure 1). Since attack on the substrate is not possible in the presence of a H-bonding interaction as per pathways I and III, these pathways start from the higher energy *trans* isomer, while pathway II, which involves heterolytic cleavage of the O···O bond, starts from the low-energy *cis* isomer. Thus, for both pathways I and III, there is an energy penalty of 19.9 kJ/mol compared to pathway II.

Scheme 1 also depicts the initial transition state which is involved in the attack of substrate with the $\mathbf{1}_{trans}$ species. A complete schematic for the mechanism of *ortho*-hydroxylation by $\mathbf{1}_{trans}$ is given in Scheme S1. Pathway I is bifurcated into pathways Ia and Ib, as either the proximal (Ia) or the distal (Ib) oxygen atom of the −OOH species can attack the substrate.[9e,50] The computed first transition state in pathway Ia is found to be at 115.8 kJ/mol on the sextet surface ($^{6}\mathbf{I}_{a}$-*ts1*), while for Ib, the barrier height is found to be much higher (154.0 kJ/mol). The optimized structures of these transition states are given in Figure 1c,d. The $\mathbf{I}_{a}$-*ts1* is a six-membered transition state where the Fe−O1 bond length elongates to 2.166 Å from 1.884 Å in the reactant. The O−O bond is only slightly elongated in the

dx.doi.org/10.1021/ja307077f | J. Am. Chem. Soc. 2013, 135, 4235−4249

transition state (1.498 Å vs 1.476 Å), and the O−C bond is partially formed. However, for Ib the structural details are drastically different, with the Fe−O bond shortening to 1.787 Å and the O−O bond elongating to 1.871 Å. This indicates that in I_b-*ts1* transition state, the O−O bond is already cleaved. The differential electrophilicity (spin densities on the proximal and distal oxygens are 0.417 and 0.077, respectively, on the reactant species $^6\mathbf{I}_{trans}$) of the two oxygen atoms lead to this large change in energetics/structures. Considering large barrier heights encountered for these transition states (and others in this mechanistic path; see Figures S34 and S35 for the computed PES), and comparing these energetics to those of pathways II and III (see below), we can safely ignore the possibility of Fe^{III}−OOH as a potential oxidant in this reaction. This is also in line with the kinetic experiments performed for the *ortho*-hydroxylation reaction, where self-decay rather than a direct attack of the Fe^{III}−OOH species is proposed.[3g,h]

Pathway II: Formation of [(TPA)Fe^{V}=O]$^{2+}$ Intermediates. Initially O···O cleavage is assumed to take place. The O···O bond can cleave homolytically or heterolytically, and in several instances it has been shown that the presence of protons aids heterolytic cleavage. In pathway II, to probe the possibility of the Fe^{V}=O species as the potential oxidant, we take $\mathbf{1}_{cis}$ as the reactant. As the hydrogen atom of the −COOH group is in H-bonding interaction, the O···O cleavage will be aided by the presence of protons. The computed PES for this reaction is shown in Figure 2. The barrier height is computed to be 69.9

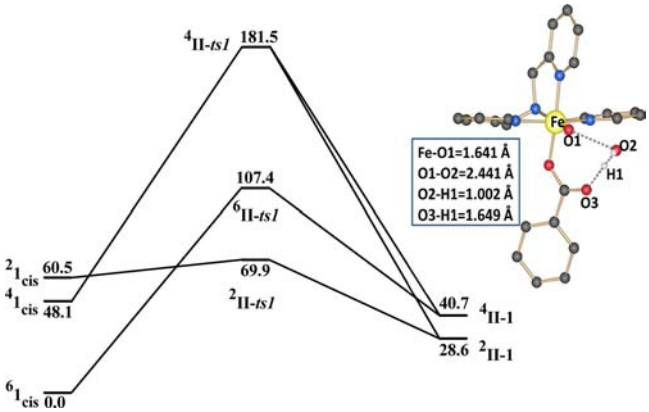

Figure 2. B3LYP-D3-computed potential energy surface (Δ*G* in kJ/mol) for the O···O cleavage starting from $\mathbf{1}_{cis}$ species along with ^{2}II-*ts1* with selected structural parameters. Fe−O1, O1−O2, O2−H1, and O3−H1 distances (Å) for ^{6}II-*ts1* (^{4}II-*ts1*): 1.678 (1.720), 1.964 (1.783 Å), 1.631 (1.599), and 1.015 (1.017), respectively.

and 107.4 kJ/mol for the doublet (^{2}II-*ts1*) and sextet (^{6}II-*ts1*) spin surfaces, respectively. The doublet surface is found to have the lowest barrier height among the three spin states computed (see Figure 2). Since the sextet surface is estimated to be the ground state for the reactant, this demands a spin-crossover. Here we have computed the MECP between the sextet and doublet surface (see Figures S5 and S36 and related discussion). Our calculations suggest that this crossing is viable. In the transition state ^{2}II-*ts1*, the O···O bond elongates to 2.441 Å, compared to 1.493 Å in the reactant, and the Fe−O bond shortens to 1.641 Å, indicating the development of Fe=O character. In the transition state, clearly the O···O bond is nearly broken, as the distal oxygen has already formed H_2O by accepting a proton from the benzoic acid. However, ^{6}II-*ts1* is very different, as here the O···O bond is still intact, with only partial migration of the proton from the benzoic acid. Thus, the low-spin transition state can be termed as product-like, while the other two transition states are reactant-like.

The spin density distribution of the ^{2}II-*ts1* transition state (see Figure S37) indicates clearly that the O···O bond cleaves heterolytically, as O1 and O2 have disproportionate spin distributions (0.574/0.877 vs 0.574/−0.268 for homolytic vs heterolytic). This leads to the formation of Fe^{V}=O (^{2,4}II-**1**), which is found to be slightly endothermic in nature (28.6 kJ/mol). The Fe^{V}=O has a doublet ground state, with the quartet lying only 12.1 kJ/mol higher in energy (see Figure 2). The computed ground state, the energy gap, and the structure are consistent with previous theoretical and experimental reports.[19,34a,51] The computed Fe−O bond length agrees with the reported X-ray structure of Fe^{V}=O species with slightly different ligand architecture (see Table S6, where comparisons to available experimental structures are made; also see Figure S38 for spin density plot and relevant discussion).

In the forthcoming steps, we explore the *ortho*-hydroxylation mechanism where the putative Fe^{V}=O intermediate is expected to trigger the catalytic reaction. There are two possible pathways by which the hydroxylation can take place. In the first path (pathway IIa), the ferryl oxygen activates the C−H bond of the benzoic acid via II_a-*ts2* (see Scheme 2), where essentially the oxygen abstracts the hydrogen atom, forming an Fe^{III}−radical intermediate ($^{2,4,6}II_a$-**2**). This radical intermediate subsequently undergoes −OH rebound via II_a-*ts3*, leading to *ortho*-hydroxylated product. In the second possible pathway (pathway IIb), electrophilic attack of the ferryl oxygen on the aromatic ring is assumed (via IIb-*ts2*) followed by the formation of a different Fe^{III}−radical intermediate (II_b-**2**) where the benzene ring is essentially dearomatized. In the subsequent step, hydrogen migration takes place from the sp^3-hybridized carbon to the oxo group (via II_b-*ts3*), leading to *ortho*-hydroxylated product.

Pathway IIa. The Fe^{V}=O species, although it has been characterized thoroughly on only a few occasions,[5,19,23a,25b,52] has been proposed as the possible oxidant both in heme and non-heme chemistry.[19,49f,52b,53] C−H activations by non-heme Fe^{V}=O compounds are documented in the literature.[49b,52b,d] The computed PES for pathway IIa is shown in Figure 3. The optimized structure of the transition state (^2II_a-*ts2*) is shown in Figure 4a. The barrier height in the doublet surface for the abstraction is estimated to be 45.5 kJ/mol, while a much higher barrier has been calculated for the quartet surface (122.6 kJ/mol).[54] As expected, the approach of the hydrogen atom leads to elongation of the Fe−O bond both in the doublet and in the quartet surface. The newly forming O1−H1 bond is partially formed, while the C1−H1 bond is partially broken, revealing that the transition state is somewhat in between the reactant and the product. A large difference in the computed barrier heights is reflected in the estimated spin density (see Figure S39), where the doublet and the quartet ferryl oxygen spin densities are grossly different in the transition state (0.974 to 0.020 for doublet, see Table S7). In the next step, the Fe^{IV}−radical intermediate form where the Fe−O bond further elongates and the −OH bond forms completely. A sizable spin density is detected at the aromatic ring, indicating the formation of a radical-type intermediate. This intermediate is exothermic with respect to the reactant, with the ^6II_a-**2** being the ground state. In the next step, −OH rebound takes place via II_a-*ts3* transition state. Here, the lowest barrier height is estimated to be 6.3 kJ/mol on the ^6II_a-*ts3* surface, and the

dx.doi.org/10.1021/ja307077f | *J. Am. Chem. Soc.* 2013, 135, 4235−4249

Scheme 2. Adapted DFT Mechanism for *ortho*-Hydroxylation by Putative Fe^{V}=O Species

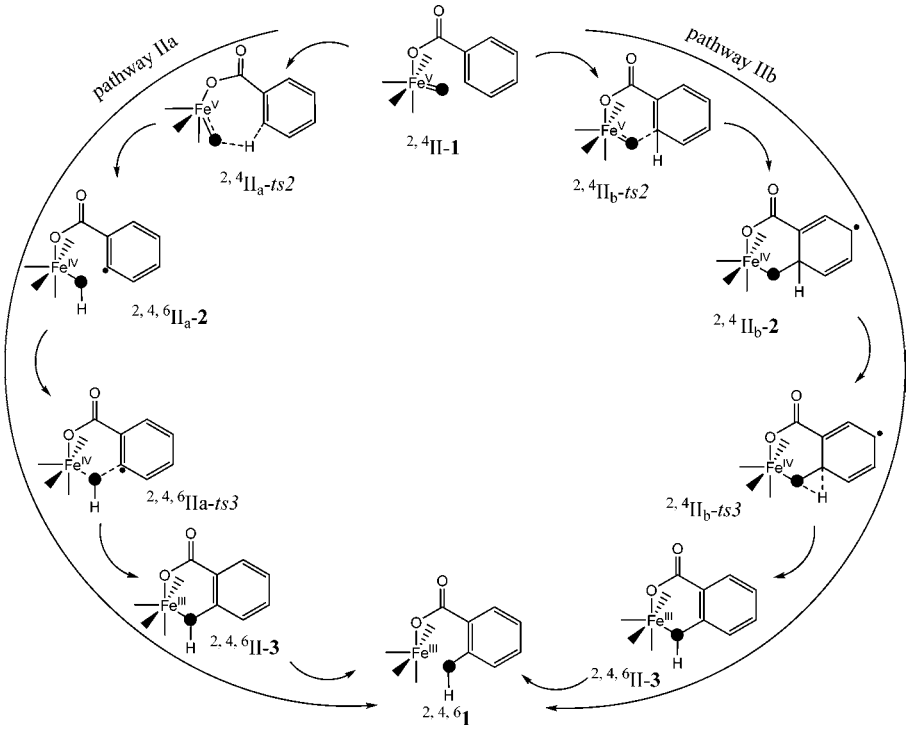

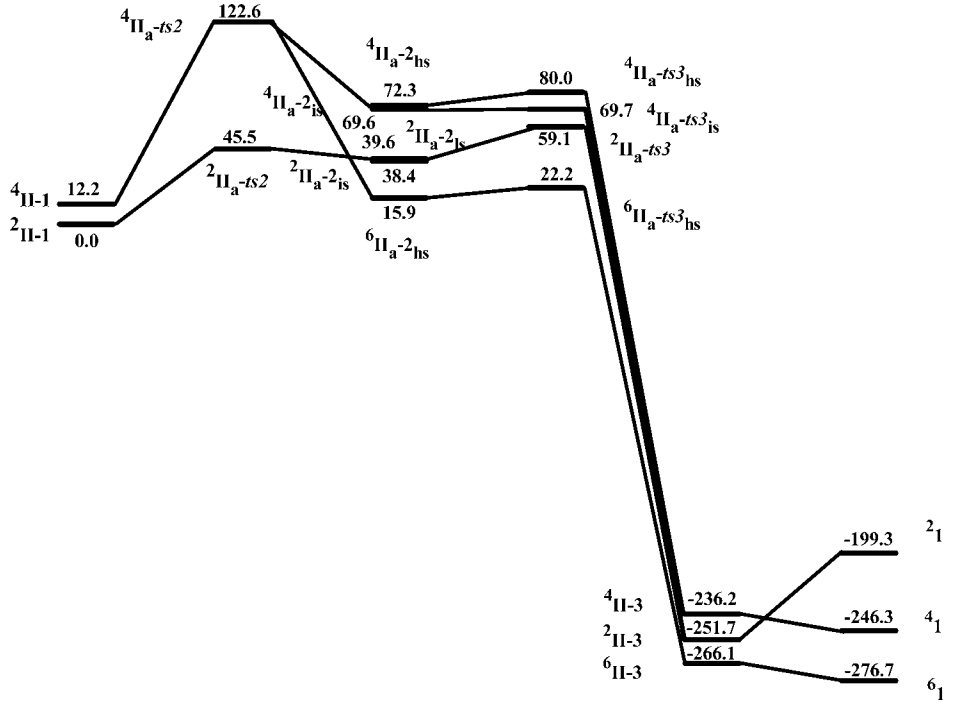

Figure 3. B3LYP-D3-computed potential energy surface (ΔG in kJ/mol) for pathway IIa.

newly forming O1−C1 bond is exceptionally long (3.675 Å). However, frequency and IRC calculations confirm the true nature of this transition state. The transition states calculated on other surfaces are energetically higher (see Figure 3). In the next step, the O1−C1 bond completes, leading to an intermediate which is common to both pathways a and b (see Figure 4b). For this intermediate the Fe−O bond is 2.114 Å, indicating the readiness of this bond to cleave to yield the *ortho*-hydroxylated product. The thermodynamic formation of this intermediate is estimated to be −266.1 kJ/mol, indicating facile formation of this intermediate. The large exothermicity of the product is due to the gain of aromaticity which was lost during the course of the reaction.[55] In the next step the Fe−O bond cleaves, leading to the formation of the final product, which then is in turn more stable than the intermediate. A large thermodynamic stability of this final product indicates that the forthcoming catalytic cycles will be aided by a gain in energy, as demonstrated based on the two-state reactivity principle.[34a,56]

dx.doi.org/10.1021/ja307077f | *J. Am. Chem. Soc.* 2013, 135, 4235−4249

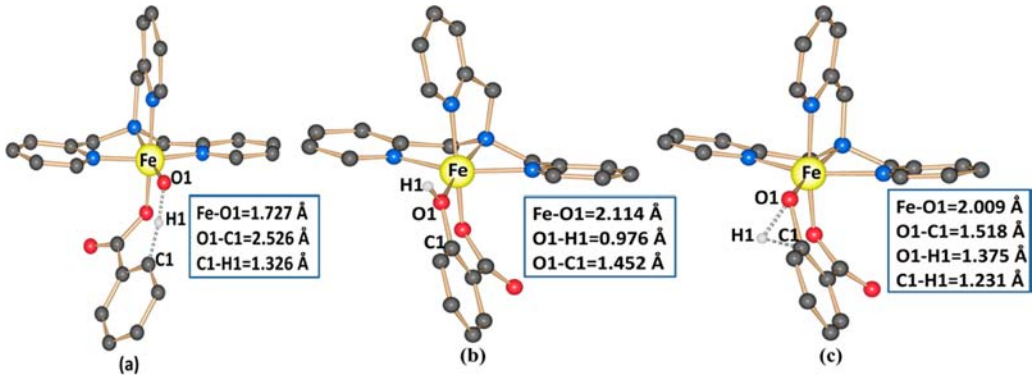

Figure 4. B3LYP-D3-optimized structures with selected structural parameters: (a) $^{2}II_{a}$-*ts2*, where Fe−O1, O1−H1, and C1−H1 (Å) for $^{4}II_{a}$-*ts2* are 1.750, 1.201, and 1.332; (b) $^{6}II_{a}$-3, where Fe−O1, O1−H1, and O1−C1 (Å) for $^{4}II_{a}$-3 ($^{2}II_{a}$-3) are 2.216 (2.022), 0.976 (0.978), and 1.442 (1.460), respectively; and (c) $^{6}II_{b}$-*ts3*, where Fe−O1, O1−H1, and C1−H1 (Å) for $^{4}II_{b}$-*ts3* ($^{2}II_{b}$-*ts3*) are 2.051 (1.948), 1.401 (1.397), and 1.219 (1.224), respectively.

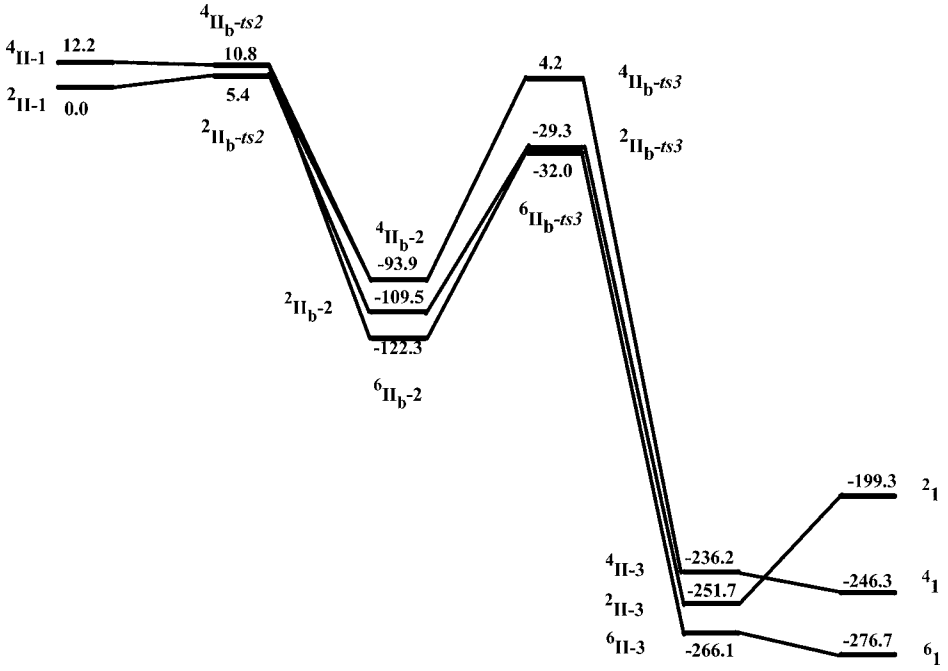

Figure 5. B3LYP-D3-computed potential energy surface (ΔG in kJ/mol) for pathway IIb.

Pathway IIb. In pathway IIb, the product formation takes place via two transition states and two intermediates (see Scheme 2). The pathway proceeds with the electrophilic attack of the ferryl oxygen on the *ortho* carbon atom of the benzoic acid via II_{b}-*ts2*. The barrier height is estimated to be just 5.4 kJ/mol on the doublet and 10.8 kJ/mol on the quartet surface. The Fe−O bond elongates significantly on both surfaces, and the newly forming O1−C1 bond is partially formed on both surfaces (2.656 Å for $^{2}II_{b}$-*ts2* and 1.951 Å for $^{4}II_{b}$-*ts2*). The spin density plot of the $^{2}II_{b}$-*ts2* is shown in Figure S40 (see also Table S8). The ferryl oxygen gains significant spin density compared to the Fe^{V}═O reactant at the same time the Fe atom has pretty much the same spin density on both the reactant and the transition state. This suggests formation of an oxyl radical at the transition state; a similar case has been reported for a non-heme Fe^{IV}═O-catalyzed C−H activation reaction.[57]

In the next step, the O1−C1 bond completes, leading to the formation of a radical intermediate. There are five possible spin-coupled intermediates; however, we are unable to converge two intermediates ($^{4}II_{b}$-**2**$_{hs}$ and $^{2}II_{b}$-**2**$_{is}$). The $^{6}II_{b}$-**2**$_{hs}$ intermediate is found to be the ground state, and the formation of this intermediate is exothermic by 122.3 kJ/mol. As expected, the Fe−O bond elongates further, and the O1−C1 bond formation completes at this intermediate. As sextet is the ground state for the intermediate while doublet is the lowest energy first transition state, a MECP from the doublet to the sextet surface is expected, and this has also been computed to be feasible (see Figure S41 for geometry and discussion). A large spin−orbit interaction is expected for the Fe^{V}═O doublet transition states due to nearly degenerate d_{xz} and d_{yz} orbitals.[14j,58] This is likely to drive the crossover from doublet to sextet surface after the formation of the transition state. In the next step after the formation of the radical intermediate via II_{b}-*ts3*, hydrogen migration to the ferryl oxygen takes place (see Figure 4c). For this transitions state again, sextet is found to be the lowest with the estimated barrier height of 90.3 kJ/mol. Although the barrier height for this process seems to be high from the reactant energy the process, this step is barrierless, as the radical

dx.doi.org/10.1021/ja307077f | J. Am. Chem. Soc. 2013, 135, 4235−4249

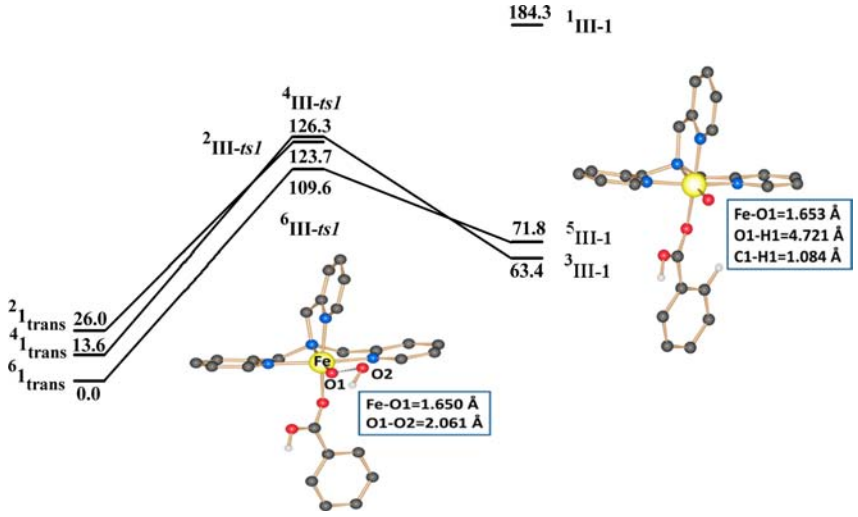

Figure 6. B3LYP-D3-computed potential energy surface for the O···O cleavage starting from $\mathbf{1}_{trans}$ species.

intermediate is significantly stabilized (see Figure 5). At the transition state the Fe−O bond elongates further (^{6}II$_{b}$-*ts3*), and the hydrogen migrates to the middle position between the C1 and O1 (see Figure 4c). The formation of the common radical intermediate for both pathways IIa and IIb is the next step. The structure and the energetics of these species and the formation of the final product were already discussed for pathway IIa.

Pathway III: Formation of [(TPA)Fe^{IV}=O]$^{2+}$ Intermediates. Much like in pathway II, in pathway III also initially the O···O cleavage is assumed to take place. In this path, we are aiming to generate a transient Fe^{IV}=O species, and therefore we have taken $\mathbf{1}_{trans}$ as the reactant and probed the O···O bond cleavage. For $\mathbf{1}_{trans}$ species, sextet is found to be the ground state, with the doublet and the quartet lying at 13.6 and 26.0 kJ/mol. The O···O bond cleavage transition state has been computed in all three PESs, and the computed profile is shown in Figure 6. The barrier height for the O···O cleavage is computed to be 123.7, 109.6, and 126.3 kJ/mol for the doublet (^{2}III-*ts1*), sextet (^{6}III-*ts1*; see Figure 6), and quartet (^{4}III-*ts1*) spin surfaces. To understand whether the O···O bond is cleaving homolytically or heterolytically, the spin density of the ^{6}III-*ts1* was analyzed, and this indicates (0.574 and 0.877 on proximal and distal oxygens, respectively, and see spin density plot in Figure S42) that the O···O bond is cleaving homolytically. Homolytic cleavage of the O···O bond results in formation of the putative Fe^{IV}=O species (^{5,3,1}III-**1**). For this Fe^{IV}=O (III-**1**) species, a triplet state is found to be the ground state, with the quintet and the singlet 8.4 and 120.9 kJ/mol higher in energy, respectively. The results are consistent with the experiments, where triplet is determined to be the ground state from the Mössbauer spectroscopy and other spectroscopic measurements for species III-**1**.[4a,25d,34a,41a,b,59] The optimized structure of ^{3}III-**1** is shown in Figure 6. For ^{3}III-**1** species, the Fe−O bond length is computed to be 1.653 Å, and this is consistent with the experimental data reported for other Fe^{IV}=O complexes (see Table S6).[48b,59a] Thermodynamically, the formation of this species is found to be endothermic by 63.4 kJ/mol (for ^{3}III-**1**). Although a different computational protocol and slightly different models were employed, the energetics computed here are comparable to those found in the previous theoretical studies.[14j,49a]

In the forthcoming steps, we explore the *ortho*-hydroxylation mechanism where the putative Fe^{IV}=O intermediate is expected to trigger the catalytic reaction. Similar to the Fe^{V}=O species, there are two possible pathways. First, hydroxylation can take place via C−H activation (pathway IIIa) by III$_{a}$-*ts2* transition state (see Figure 7a). In the second possible pathway (pathway IIIb), an electrophilic attack of the ferryl oxygen on the aromatic ring is assumed (via III$_{b}$-*ts2*), similar to pathway IIb (see Scheme S2 for a detailed mechanistic scheme).

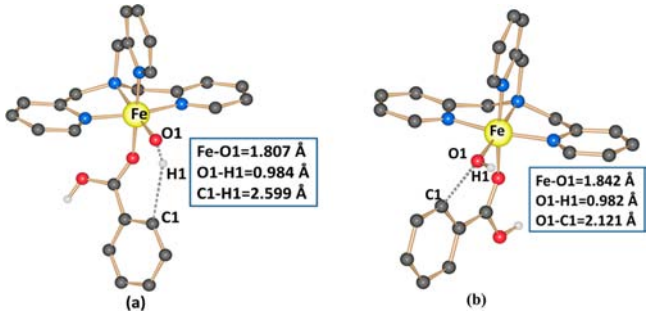

Figure 7. B3LYP-optimized structures with selected structural parameters: (a) ^{3}III$_{a}$-*ts2*, where Fe−O1, O1−H1, and C1−H1 (Å) for ^{1}III$_{a}$-*ts2* (^{5}III$_{a}$-*ts2*) are 1.804 (1.785), 1.208 (1.038), and 1.253 (1.636), respectively; (b) ^{3}III$_{a}$-*ts3*$_{ls}$, where Fe−O1, O1−H1, and O1−C1 (Å) for ^{7}III$_{a}$-*ts3* (^{5}III$_{a}$-*ts3*$_{hs}$) [^{5}III$_{a}$-*ts3*$_{is}$] {^{3}III$_{a}$-*ts3*$_{is}$} ⟨^{1}III$_{a}$-*ts3*⟩ are 1.946 (1.799) [1.844] {1.842} ⟨1.817⟩, 0.980 (0.970) [0.981] {0.982} ⟨0.980⟩, and 1.769 (2.913) [2.343] {2.121} ⟨2.439⟩, respectively.

Pathway IIIa. The computed geometries are given in Figure 7, while the computed PES is shown in Figure 8. The computed barrier height for the triplet surface is 115.7 kJ/mol (see Figure 7a), while for the quintet it is estimated to be 174.5 kJ/mol. The Fe−O bond in III$_{a}$-*ts2* elongates to 1.807 and 1.785 Å for triplet and quintet surfaces, respectively, compared to their corresponding bond lengths in the Fe^{IV}=O reactant. In the next step, a radical intermediate forms.[2c,59] Considering the exchange interaction between the Fe^{III} and the radical center, there are six possible spin-state energetics. Radical intermediate (see Table S9 for orbital labeling) formation is found to be endothermic in nature, and among the six spin states modeled, ^{7}III$_{a}$-**2** is found to be the lowest in energy, with ^{3}III$_{a}$-**2**$_{ls}$ lying 36.7 kJ/mol higher. In the next step, −OH rebound to the radical center takes place (see in Table S10) via ^{1,3,5,7}III$_{a}$-*ts3*,

dx.doi.org/10.1021/ja307077f | J. Am. Chem. Soc. 2013, 135, 4235−4249

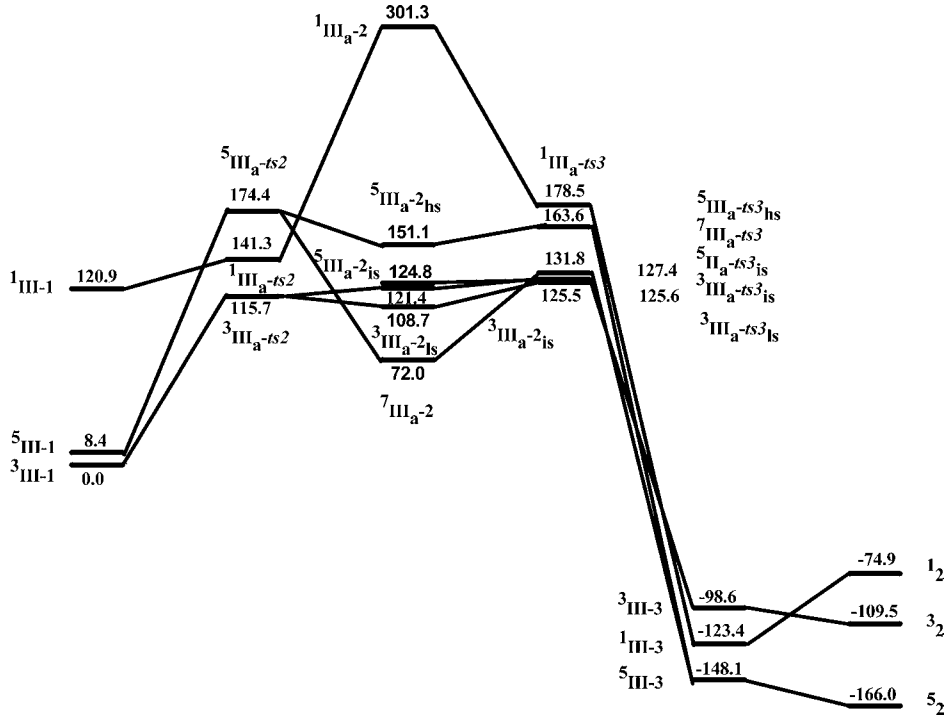

Figure 8. B3LYP-D3-computed potential energy surface (ΔG in kJ/mol) for pathway IIIa.

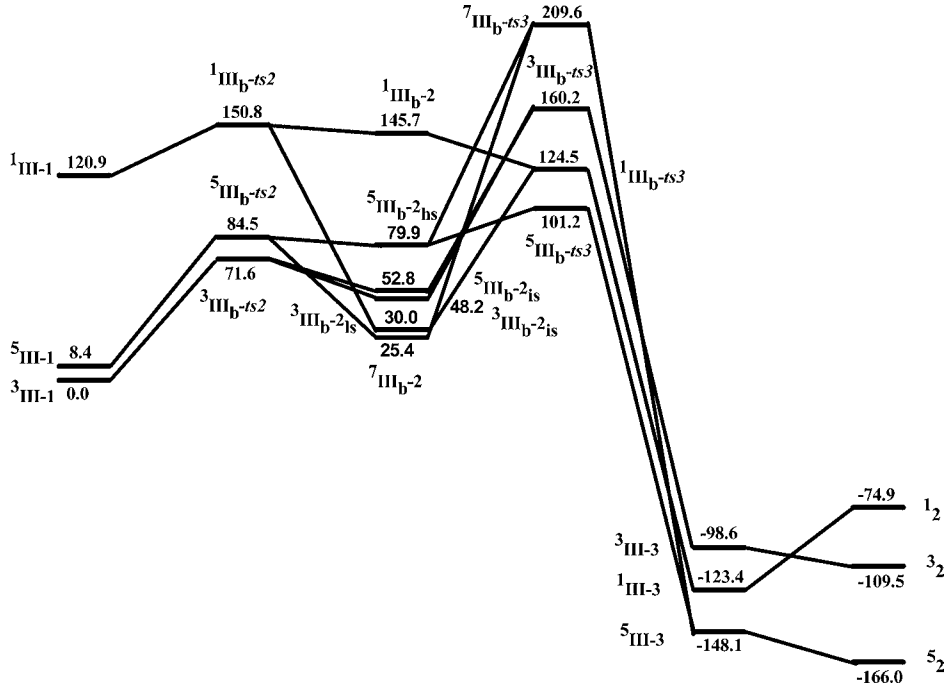

Figure 9. B3LYP-D3-computed potential energy surface (ΔG in kJ/mol) for pathway IIIb.

leading to an *ortho*-hydroxylated product; here $^{3}III_{a}$-*ts3*$_{ls}$ is found to be the lowest lying transition state. In the next step, a −OH-bound radical intermediate (III-**3**) is formed. The energetics reveals the quintet spin state is the most stable for this intermediate. Here the Fe−O bond further elongates to reach 2.173 Å, and in the next step this bond is expected to cleave, forming *ortho*-hydroxylated product. This product formation is found to be exothermic, with the quintet state being the ground state and the overall thermodynamic stabilization of −166.0 kJ/mol.

Pathway IIIb. A second scenario has been considered, with direct electrophilic attack of the ferryl oxygen into the aromatic ring by Fe^{IV}═O oxidant.[2c,30c,33a] The computed energy profile diagram for this pathway is shown in Figure 9, and optimized structures are shown in Figure 10. For the first transition state (II_{b}-*ts2*), the barrier height is estimated to be 71.6 kJ/mol on the triplet and 84.5 kJ/mol on the quintet surface, whereas the same transition state and other species having low-spin Fe configuration in the singlet surface are very high in energy. Thus, here we focus our attention on triplet and quintet

dx.doi.org/10.1021/ja307077f | J. Am. Chem. Soc. 2013, 135, 4235−4249

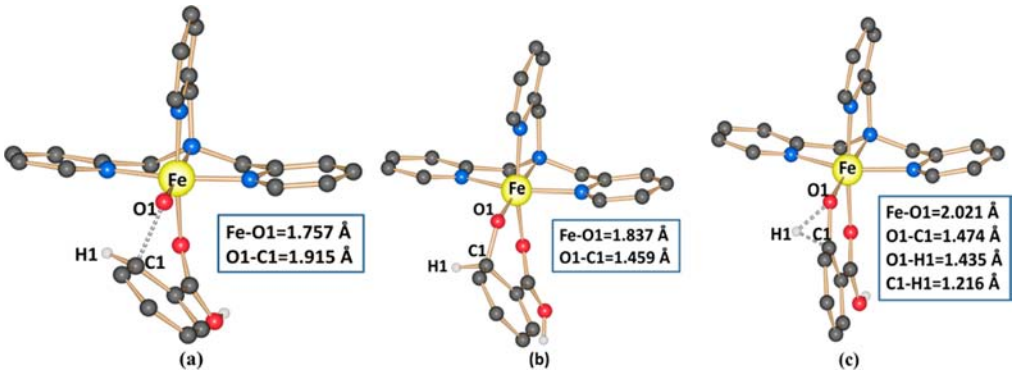

Figure 10. B3LYP-D3-optimized structures with selected structural parameters: (a) $^{3}III_{b}$-*ts2*, where Fe−O1 and O−C1 (Å) for $^{5}III_{b}$-*ts2* ($^{1}III_{b}$-*ts2*) are 1.747 (1.720) and 1.899 (2.177), respectively; (b) $^{7}III_{b}$-**2**, where Fe−O1 and O1−C1 (Å) for $^{5}III_{b}$-$\mathbf{2}_{hs}$ ($^{5}III_{b}$-$\mathbf{2}_{is}$) [$^{3}III_{b}$-$\mathbf{2}_{is}$] {$^{3}III_{b}$-$\mathbf{2}_{ls}$} ⟨$^{1}III_{b}$-$\mathbf{2}_{ls}$⟩ are 1.835 (1.817) [1.818] {1.821 Å} ⟨1.821⟩ and 1.471 (1.487) [1.476] {1.476} ⟨1.472⟩, respectively; and (c) where Fe−O1, O1−H1, and C1−H1 for $^{7}III_{b}$-*ts3* ($^{3}III_{b}$-*ts3*$_{ls}$) [$^{1}III_{b}$-*ts3*$_{ls}$] are 1.968 (2.001) [1.943], 1.190 (1.404) [1.447], and 1.370 (1.236) [1.213], respectively.

Scheme 3. Orbital Occupancy Diagrams for the H-Abstraction Processes and Corresponding Orbital Selection Rules for Predicting Transition-State Structures

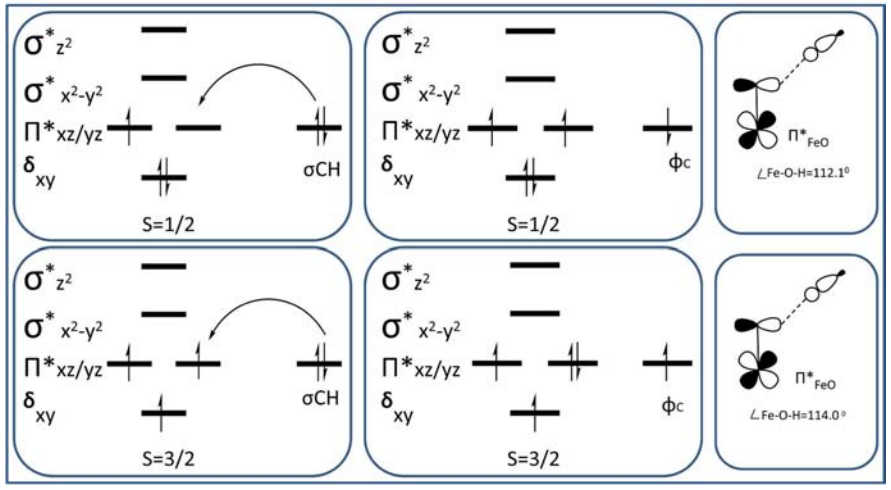

surfaces. The Fe−O distance is elongated compared to the reactant, while the newly forming O−C distance is nearly equal in both the quintet and triplet surfaces (∼1.90 Å). Similar to the pathway previously discussed, there is a significant reduction in the spin density on Fe and the ferryl oxygen atom. Unlike the previous pathway (where a large localized spin density on C was detected), the spin density on the aromatic ring is found to be strongly delocalized (see Figure S43 and Table S11). This significantly stabilizes both the transition states and the forthcoming radical intermediates compared to pathway IIIa. In the next step, the O1−C1 bond forms completely and the corresponding Fe−O bond elongates (see Figure 10b). In this radical intermediate, $^{7}III_{b}$-**2** is found to be the ground state. The formation of the radical intermediate is still endothermic compared to the reactant. The $^{5}III_{b}$-*ts3*$_{is}$ (see Figure 10c) is found to be the next step, where the hydrogen atom shuttles to the bound ferryl oxygen atom. Here the $^{5}III_{b}$-*ts3*$_{is}$ (see Figure 10c) is found to be the lowest lying transition state, and thus a spin-crossover from $^{7}II_{b}$-**2** to $^{5}II_{b}$-*ts3*$_{is}$ is expected to occur. In $^{5}III_{b}$-*ts3*$_{is}$ transition state, the C−H bond elongates to 1.216 Å, while the newly forming H1−O1 bond is 1.435 Å. The next step is the formation of the −OH bound intermediate, where both the pathways IIIa and IIIb converge to a common intermediate that eventually leads to the *ortho*-hydroxylated product.

DISCUSSION

Methodology. Use of the B3LYP functional including dispersion correction yields barrier heights markedly lower than those obtained with the conventional B3LYP functional, and this highlights the importance of a dispersion-corrected functional for understanding the reaction mechanism.

Heterolytic vs Homolytic O···O Cleavage. The possibility of Fe^{III}−OOH species directly hydroxylating the substrate has been eliminated, as the computed barrier height for this to occur is enormously high compared to the formation of the high-valent Fe species which triggers the reaction.

Our study indicates that the *trans*-Fe^{III}−OOH undergoes exclusive O···O homolysis, generating the Fe^{IV}=O oxidant, while the *cis*-isomer undergoes exclusive O···O heterolysis, leading to the formation of the Fe^{V}=O oxidant. Since the *cis* isomer is stabilized by 19.9 kJ/mol, the conversion of *cis* to *trans* under ambient conditions is likely. A relaxed scan performed also supports this argument (see Figure S44 and related discussion).

The coordinated benzoic acid aids the heterolytic cleavage of the O···O bond (69.9 kJ/mol vs 109.6 kJ/mol for heterolytic vs

dx.doi.org/10.1021/ja307077f | J. Am. Chem. Soc. 2013, 135, 4235−4249

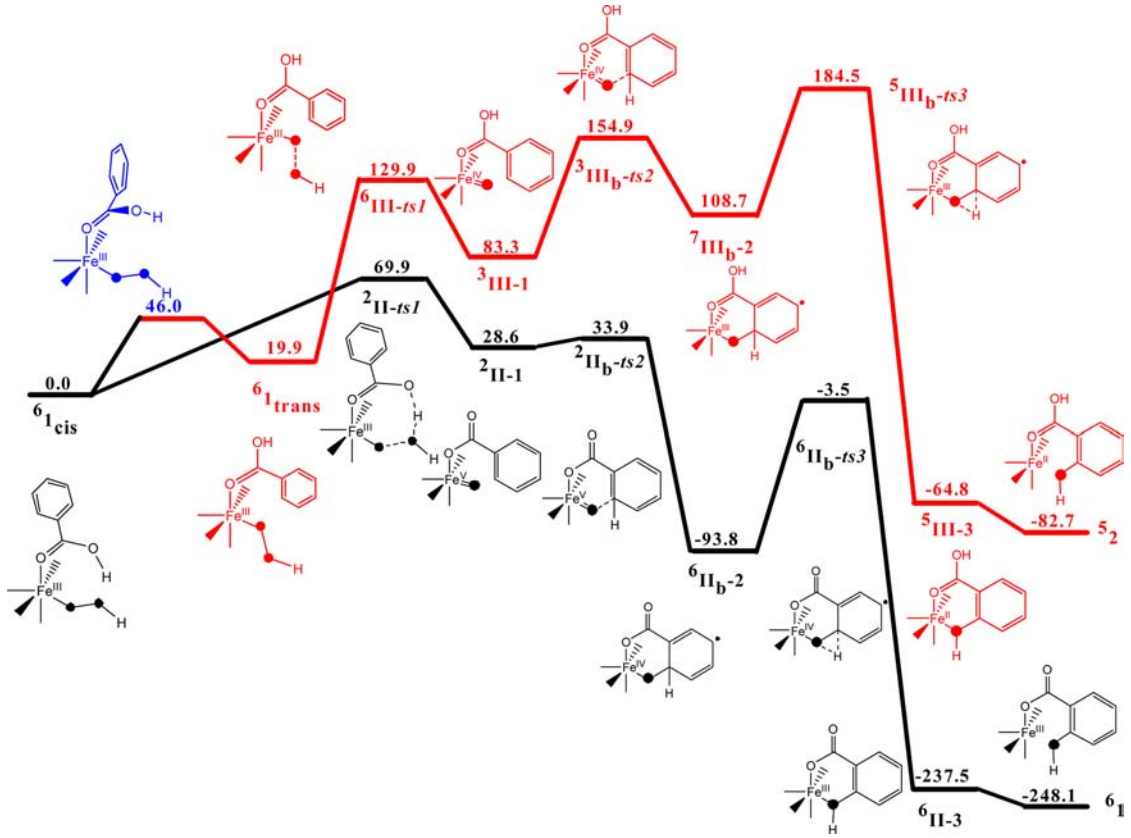

Figure 11. Comparative energy level diagram (ΔG in kJ/mol) for the *ortho*-hydroxylation of aromatic compounds by Fe^{IV}=O (red) and Fe^{V}=O (black) oxidants.

homolytic cleavage; also see Scheme S3). The Fe^{V}=O formation is also favored thermodynamically compared to the corresponding Fe^{IV}=O species by a margin of 34.8 kJ/mol. The facts that Fe^{V}=O is a vigorous oxidant compared to Fe^{IV}=O[3g,19,49a,b] and its formation is substantiated by the presented energetics indicate Fe^{V}=O is the oxidant which triggers this catalytic transformation.

As the O···O cleavage is aided by protons, a viable heterolytic cleavage demands at least two coordination vacancies at the catalytic site. Thus, with a pentadentate ligand system, such a conversion is not expected to be viable, and here the reaction may proceed via Fe^{IV}=O species as reported recently with pentadentate *N*-R-*N*,*N*′,*N*′-tris(2-pyridylmethyl)ethane-1,2-diamine ligand system.[24]

C−H Activation vs Electrophilic Attack. Two different mechanistic proposals have been given, and both Fe^{IV}=O and Fe^{V}=O have been considered as oxidant in these pathways. Two different pathways have been modeled for each of the oxidants. In the case of the Fe^{IV}=O oxidant (pathway IIIa), both the C−H activation (115.7 kJ/mol) and the −OH rebound step (53.5 kJ/mol) have significant barriers, with the C−H activation being the rate-determining step (rds). A very small triplet and quintet gap (8.4 kJ/mol) indicates that the reactivity of Fe^{IV}=O should be vigorous; however, the barrier heights computed are very large.

Generally the rds for the Fe^{IV}=O oxidant is substantially smaller in the quintet surface compared to the triplet surface.[2c,25c,61] In the quintet surface, there are two possible mechanisms by which the C−H activation takes place: (i) via the participation of σ-type Fe-d_{z^2} orbital or (ii) via participation of π-type Fe-$d_{xz/yz}$ orbitals. The first mechanism demands the Fe−O···H angle to be ca. 180°, while for the second, it should be around 120°. It is the first mechanism by which the energy lowering for quintet has been witnessed in the majority of cases.[62] In our case, this substantial lowering of barrier height due to the low-lying quintet is not observed; in fact, the triplet transition state is found to be low-lying. This is essentially due to the fact that the benzoic acid coordinates to the Fe atom, and this coordination restricts the Fe−O···H angle (see Scheme 3); thus, the reaction proceeds via a triplet transition state.

In the second mechanism (pathway IIIb), we expect an electrophilic attack of the ferryl oxygen on the aromatic ring. Here again the initial O_{ferryl}−$C_{aromatic}$ bond formation is found to be the rds (71.6 kJ/mol), while H-migration also has a significant barrier (75.8 kJ/mol). There is no substantial lowering of the barrier heights due to the low-lying quintet surface for the same reason that we have outlined above. Between the two pathways, our calculations predict electrophilic attack (pathway IIIb) to be energetically favorable over C−H activation (pathway IIIa). The HOMOs of the two transition states (^{3}III$_a$-*ts2* and ^{3}III$_b$-*ts2*) are shown in Figure S45a,b. It is apparent from this figure that pathway IIIa involves activation of the σ_{CH} bond while pathway IIIb involves $\pi_{C=C}$ orbitals. Apparently due to the variation of σ_{C-H} and $\pi_{C=C}$ bond dissociation energies, electrophilic attack is found to be the favored pathway.

Likewise, Fe^{V}=O has been studied considering pathway IIa (C−H activation) and pathway IIb (electrophilic attack). Larger exchange stabilization due to the involvement of spin state with higher multiplicity, as observed for the Fe^{IV}=O oxidant, is also true for the Fe^{V}=O oxidant (see Scheme 3).[52c,63] In pathway IIa, the rds is found to be the initial C−H

dx.doi.org/10.1021/ja307077f | *J. Am. Chem. Soc.* 2013, 135, 4235−4249

activation (45.5 kJ/mol) step, while the second −OH rebound has negligible barrier height. For pathway IIb, the rds is found to be the $O_{ferryl}-C_{aromatic}$ bond formation (5.4 kJ/mol), with the second step essentially barrierless from the reactant. Between these two pathways, electrophilic attack is favored energetically. The HOMO of the ^2II_b-*ts2* is shown in Figure S45c. Quiet interestingly, the Fe orbitals involved in the electrophilic attack between the Fe^{IV}=O and the Fe^{V}=O are different, with ($\pi_{xz}-p_y$)* antibonding orbital in Fe^{IV}=O and ($\pi_{xz}-p_y$) bonding orbital in Fe^{V}=O (see Figure S45b,c).

Between pathways IIb and IIIb, apparently pathway IIb is favored energetically by 66.2 kJ/mol (5.4 vs 71.6 kJ/mol), and in addition to that, considering a significant barrier height for the forthcoming steps in pathway IIIb and a barrierless step in pathway IIb, it is straightforward to conclude that the reaction prefers Fe^{V}=O oxidant and proceeds via pathway IIb. The thermodynamic formation energy of the product is also strongly inclined towards the Fe^{V}=O oxidant.

Overall, a comparative energy profile diagram incorporating all energy costs starting from the most stable *cis*-Fe^{III}−OOH and showing only the lowest energy states for both the transition state and the intermediates is shown in Figure 11. From the computed PES, it is apparent that the Fe^{V}=O formation is energetically favored over the Fe^{IV}=O species. Furthermore, the Fe^{V}=O species undergoes an electrophilic attack on the aromatic carbon, which eventually leads to the *ortho*-hydroxylated product.

Correlation to Experiments. Our results are fully supported by the experiments where Fe^{V}=O has been proposed as the oxidant for the *ortho*-hydroxylation of benzoic acid and its substituted derivative.[3g,h,22] The kinetic experiments performed for a slightly different ligand[3h] suggest that the Fe^{III}−OOH does not directly attack the aromatic ring, and its decay to another species was observable. This is supported by our calculations where prohibitively high barrier heights were computed for Fe^{III}−OOH as an oxidant. In situ generated Fe^{IV}=O with H_2O_2 and acetic acid is found not to hydroxylate benzene; also direct generation of the Fe^{IV}=O complex using 2-iodoxybenzoic acid did not effect the reactions. This experiment suggests that Fe^{IV}=O is also an unlikely oxidant in this chemistry, supported by our calculations where a substantial barrier height for the O−C bond formation for Fe^{IV}=O species has been estimated, with the second step of H-migration also adding a significant energy penalty. This essentially suggests that the Fe^{IV}=O is unlikely to *ortho*-hydroxylate aromatic compounds.

The O−O bond of Fe^{III}−OOH is found cleave heterolytically, as evidenced by the product analysis of the reaction of Fe^{III}−OOH with organic peroxide 2-methyl-1-phenyl-2-propyl hydroperoxide (MPPH).[3h] This correlates strongly with our computed O···O cleavage pathway energetics, where the Fe^{V}=O species is preferred. The measured kinetic isotopic effect reveals a small inverse kinetic isotopic effect value (k_H/k_D = 0.8),[3h] indicating a change in hybridization at the aromatic carbon and hence suggesting the electrophilic attack is the possible pathway; our computations also strongly support this hypothesis where the electrophilic attack pathway is found to be favored by all oxidants.

CONCLUSIONS

DFT calculations have been performed to explore the mechanism of *ortho*-hydroxylation of aromatic compounds with an Fe(II) precursor complex. We have explored various reaction pathways possible in the course of *ortho*-hydroxylation. DFT calculations clearly reveal that Fe^{III}−OOH is a sluggish oxidant, as both proximal and distal oxygens have prohibitively large barriers to carry out aromatic hydroxylation. The possibility of cleaving the O···O bond of the Fe^{III}−OOH species homolytically and heterolytically by generating different high-valent oxidants has been explored. Our calculations reveal that the O···O bond in Fe^{III}−OOH species undergoes heterolytic cleavage to form a transient Fe^{V}=O oxidant. This high-valent species triggers the catalytic reaction, and two different mechanistic schemes are outlined and studied. From the computed PES, it is apparent that the formation of the Fe^{V}=O is energetically favored over the Fe^{IV}=O species. The Fe^{V}=O species undergoes an electrophilic attack on the aromatic carbon which eventually leads to the *ortho*-hydroxylated product. Although the Fe^{IV}=O species has been proposed as the oxidant for various oxidation reactions, in this particular reaction studied, the coordination of benzoic acid to the Fe strongly favors heterolytic cleavage of the O···O bond of the Fe^{III}−OOH species (acid-assisted cleavage). This coordination also leads to very large barrier heights for the Fe^{IV}=O species to attack the aromatic ring. This invariably suggests that, by tuning the axial ligation, one can also alter the oxidant to fine-tune the reactivity. Our results are in agreement with the experimental data on the subject. Other research groups have also reported Fe^{V}=O as the potential oxidant in the *ortho*-hydroxylation reaction.

ASSOCIATED CONTENT

Supporting Information

Method assessment with computed PES with B3LYP, M06-2X, wB97XD, B97D, TPSSh, OLYP, and MP2 methods along with a detailed discussion on computed energetics and the performance of different functionals on spin-state splitting and estimation of barrier heights; tables summarizing the energetics computed with different functionals; PESs computed with and without incorporating the free energy corrections; mechanistic scheme for pathway Ia and the corresponding computed PES; computed MECP geometries and the corresponding PES; various computed spin density plots; tables containing computed spin densities values on selected atoms for all the species; mechanistic schemes for pathways Ia, IIIa, and IIIb; relaxed scan performed on species **1**; schematic diagram illustrating the homo- vs heterolytic cleavage; complete ref 31. This material is available free of charge via the Internet at http://pubs.acs.org.

AUTHOR INFORMATION

Corresponding Author

rajaraman@chem.iitb.ac.in

Notes

The authors declare no competing financial interest.

ACKNOWLEDGMENTS

Dedicated to Prof. P. Venuvanalingam on his 60th Birthday. G.R. acknowledges financial support from the Government of India through Department of Science and Technology (SR/S1/IC-41/2010; SR/NM/NS-1119/2011) and generous computational resources from Indian Institute of Technology-Bombay. A.A. thanks CSIR for a JRF fellowship. We also thank the anonymous reviewers for their helpful suggestions.

REFERENCES

(1) (a) Sheldon, R. A.; Kochi, J. K. *Metal-Catalyzed Oxidations of Organic Compounds*; Academic Press: New York, 1981. (b) Punniyamurthy, T.; Velusamy, S.; Iqbal, J. *Chem. Rev.* **2005**, *105*, 2329.

(2) (a) Walling, C.; Johnson, R. A. *J. Am. Chem. Soc.* **1975**, *97*, 363. (b) Sawyer, D. T.; Sobkowiak, A.; Matsushita, T. *Acc. Chem. Res.* **1996**, *29*, 409. (c) de Visser, S. P.; Oh, K.; Han, A.-R.; Nam, W. *Inorg. Chem.* **2007**, *46*, 4632.

(3) (a) Mehn, M. P.; Fujisawa, K.; Hegg, E. L.; Que, L., Jr. *J. Am. Chem. Soc.* **2003**, *125*, 7828. (b) Ménage, S.; Galey, J.-B.; Dumats, J.; Hussler, G.; Seité, M.; Luneau, I. G.; Chottard, G.; Fontecave, M. *J. Am. Chem. Soc.* **1998**, *120*, 13370. (c) Furutachi, H.; Murayama, M.; Shiohara, A.; Yamazaki, S.; Fujinami, S.; Uehara, A.; Suzuki, M.; Ogo, S.; Watanabe, Y.; Maeda, Y. *Chem. Commun.* **2003**, 1900. (d) Avenier, F.; Dubois, L.; Latour, J. -M. *New J. Chem.* **2004**, *28*, 782. (e) Nielsen, A.; Larsen, F. B.; Bond, A. D.; McKenzie, C. J. *Angew. Chem., Int. Ed.* **2006**, *45*, 1602. (f) Yamashita, M.; Furutachi, H.; Tosha, T.; Fujinami, S.; Saito, W.; Maeda, Y.; Takahashi, K.; Tanaka, K.; Kitagawa, T.; Suzuki, M. *J. Am. Chem. Soc.* **2007**, *129*, 2. (g) Makhlynets, O. V.; Das, P.; Taktak, P.; Flook, M.; Mas-Ballesté, R.; Rybak-Akimova, E. V.; Que, L., Jr. *Chem.—Eur. J.* **2009**, *15*, 13171. (h) Makhlynets, O. V.; Rybak-Akimova, E. V. *Chem.—Eur. J.* **2010**, *16*, 13995.

(4) (a) Rohde, J.-U.; In, J.-H.; Lim, M. H.; Brennessel, W. W.; Bukowski, M. R.; Stubna, A.; Münck, E.; Nam, W.; Que, L., Jr. *Science* **2003**, *299*, 1037. (b) England, J.; Guo, Y.; Farquhar, E. R.; Young, V. G., Jr.; Münck, E.; Que, L., Jr. *J. Am. Chem. Soc.* **2010**, *132*, 8635. (c) Klinker, E. J.; Kaizer, J.; Brennessel, W. W.; Woodrum, N. L.; Cramer, C. J.; Que, L., Jr. *Angew. Chem., Int. Ed.* **2005**, *44*, 3690.

(5) Que, L., Jr.; Tolman, W. B. *Nature* **2008**, *455*, 333.

(6) (a) Flatmark, T.; Stevens, R. C. *Chem. Rev.* **1999**, *99*, 2137. (b) Fitzpatrick, P. F. *Biochemistry* **2003**, *42*, 14083. (c) Abu-Omar, M. M.; Loaiza, A.; Hontzeas, N. *Chem. Rev.* **2005**, *105*, 2227. (d) Foster, T. L.; Caradonna, J. P. In *Comprehensive Coordination Chemistry II*; McCleverty, J. A., Meyer, T. J, Eds.; Elsevier: Oxford, 2004; Vol. *8*, p 343. (e) Bruijnincx, P. C. A.; Van Koten, G.; Klein Gebbink, R. J. M. *Chem. Soc. Rev.* **2008**, *37*, 2716.

(7) (a) Fishman, A.; Tao, Y.; Rui, L.; Wood, T. K. *J. Biol. Chem.* **2005**, *280*, 506. (b) Sazinsky, M. H.; Bard, J.; Di Donato, A.; Lippard, S. J. *J. Biol. Chem.* **2004**, *279*, 30600. (c) Mitchell, K. H.; Rogge, C. E.; Gierahn, T.; Fox, B. G. *Proc. Natl. Acad. Sci. U.S.A.* **2003**, *100*, 3784. (d) Murray, L. J.; Lippard, S. J. *Acc. Chem. Res.* **2007**, *40*, 466.

(8) (a) Eser, B. E.; Barr, E. W.; Frantom, P. A.; Saleh, L.; Bollinger, J. M., Jr.; Krebs, C.; Fitzpatrick, P. F. *J. Am. Chem. Soc.* **2007**, *129*, 11334. (b) Krebs, C.; Fujimori, D. G.; Walsh, C. T.; Bollinger, J. M., Jr. *Acc. Chem. Res.* **2007**, *40*, 484. (c) Bollinger, J. M., Jr.; Krebs, C. *J. Inorg. Biochem.* **2006**, *100*, 586.

(9) (a) Liu, A. M.; Jin, Y.; Zhang, J. Y.; Brazeau, B. J.; Lipscomb, J. D. *Biochem. Biophys. Res. Commun.* **2005**, *338*, 254. (b) Lee, S. K.; Nesheim, J. C.; Lipscomb, J. D. *J. Biol. Chem.* **1993**, *268*, 21569. (c) Shan, X.; Que, L., Jr. *J. Inorg. Biochem.* **2006**, *100*, 421. (d) Shaik, S.; de Visser, S. P.; Kumar, D. *J. Biol. Inorg. Chem.* **2004**, *9*, 661. (e) Ogliaro, F.; de Visser, S. P.; Cohen, S.; Sharma, P. K.; Shaik, S. *J. Am. Chem. Soc.* **2002**, *124*, 2806. (f) Sharma, P. K.; de Visser, S. P.; Shaik, S. *J. Am. Chem. Soc.* **2003**, *125*, 8698. (g) Park, M. J.; Lee, J.; Suh, Y.; Kim, J.; Nam, W. *J. Am. Chem. Soc.* **2006**, *128*, 2630.

(10) (a) Meunier, B. *Chem. Rev.* **1992**, *92*, 1411. (b) Kitajima, N.; Fukui, H.; Moro-oka, Y. *J. Chem. Soc., Chem. Commun.* **1988**, 485. (c) Vincent, J. B.; Huffman, J. C.; Christou, G.; Li, Q.; Nanny, M. A.; Hendrickson, D. N.; Fong, R. H.; Fish, R. H. *J. Am. Chem. Soc.* **1988**, *110*, 6898. (d) Nam, W.; Valentine, J. S. *New J. Chem.* **1989**, *13*, 677. (e) Leising, R. A.; Norman, R. E.; Que, L., Jr. *Inorg. Chem.* **1990**, *29*, 2553. (f) Fish, R. H.; Konings, M. S.; Oberhausen, K. J.; Fong, R. H.; Yu, W. M.; Christou, G.; Vincent, J. B.; Coggin, D. K.; Buchanan, R. M. *Inorg. Chem.* **1991**, *30*, 3002. (g) Tung, H. C.; Kang, C.; Sawyer, D. T. *J. Am. Chem. Soc.* **1992**, *114*, 3445. (h) Barton, D. H. R.; Doller, D. *Acc. Chem. Res.* **1992**, *25*, 504. (i) Leising, R. A.; Kim, J.; Pérez, M. A.; Que, L., Jr. *J. Am. Chem. Soc.* **1993**, *115*, 9524. (j) Buchanan, R. M.; Chen, S.; Richardson, J. F.; Bressan, M.; Forti, L.; Morvillo, A.; Fish, R. H. *Inorg. Chem.* **1994**, *33*, 3208. (k) Lubben, M.; Meetsma, A.; Wilkinson, E. C.; Feringa, B.; Que, L., Jr. *Angew. Chem., Int. Ed. Engl.* **1995**, *34*, 1512. (l) Arends, I. W. C. E.; Ingold, K. U.; Wayner, D. D. M. *J. Am. Chem. Soc.* **1995**, *117*, 4710. (m) Ito, S.; Suzuki, M.; Kobayashi, T.; Itoh, H.; Harada, A.; Ohba, S.; Nishida, Y. *J. Chem. Soc., Dalton Trans.* **1996**, 2579. (n) Singh, B.; Long, J. R.; Papaefthymiou, G. C.; Stavropoulos, P. *J. Am. Chem. Soc.* **1996**, *118*, 5824. (o) Ménage, S.; Lambeaux, J.-M.; Fontecave, C. *J. Mol. Catal. A: Chem* **1996**, *113*, 61. (p) Nguyen, C.; Guajardo, R. J.; Mascharak, P. K. *Inorg. Chem.* **1996**, *35*, 6273. (q) Kodera, M.; Shimakoshi, H.; Kano, K. *Chem. Commun.* **1996**, 1737. (r) Mukerjee, S.; Stassinopoulos, A.; Caradonna, J. P. *J. Am. Chem. Soc.* **1997**, *119*, 8097. (s) MacFaul, P. A.; Ingold, K. U.; Wayner, D. D. M.; Que, L., Jr. *J. Am. Chem. Soc.* **1997**, *119*, 10594. (t) Kim, C.; Chen, K.; Kim, J.; Que, L., Jr. *J. Am. Chem. Soc.* **1997**, *119*, 5964.

(11) (a) Costas, M.; Mehn, M. P.; Jensen, M. P.; Que, L., Jr. *Chem. Rev.* **2004**, *104*, 939. (b) Tshuva, E. Y.; Lippard, S. J. *Chem. Rev.* **2004**, *104*, 987. (c) Hong, S.; Lee, Y. M.; Shin, W.; Fukuzumi, S.; Nam, W. *J. Am. Chem. Soc.* **2009**, *131*, 13910. (d) Yoon, J.; Wilson, S. A.; Jang, Y. K.; Seo, M. S.; Nehru, K.; Hedman, B.; Hodgson, K. O.; Bill, E.; Solomon, E. I.; Nam, W. *Angew. Chem., Int. Ed.* **2009**, *48*, 1257. (e) Lee, Y.-M.; Hong, S.; Morimoto, Y.; Shin, W.; Fukuzumi, S.; Nam, W. *J. Am. Chem. Soc.* **2010**, *132*, 10668.

(12) (a) Groves, J. T.; Nemo, T. E.; Myers, R. S. *J. Am. Chem. Soc.* **1979**, *101*, 1032. (b) Che, C. M.; Lo, V. K. Y.; Zhou, C. Y.; Huang, J. S. *Chem. Soc. Rev.* **2011**, *40*, 1950. (c) Filatov, M.; Harris, N.; Shaik, S. *Angew. Chem., Int. Ed.* **1999**, *38*, 3510. (d) Siegbahn, P. E. M. *Inorg. Chem.* **1999**, *38*, 2880.

(13) (a) Nam, W. *Acc. Chem. Res.* **2007**, *40*, 522. (b) Comba, P.; Rajaraman, G. *Inorg. Chem.* **2008**, *47*, 78. (c) Bautz, J.; Comba, P.; Laorden, C. L.; Menzel, M.; Rajaraman, G. *Angew. Chem., Int. Ed.* **2007**, *46*, 8067. (d) Comba, P.; Rajaraman, G.; Rohwer, H. *Inorg. Chem.* **2007**, *46*, 3826.

(14) (a) Solomon, E. I.; Brunold, T. C.; Davis, M. I.; Kemsley, J. N.; Lee, S. K.; Lehnert, N.; Neese, F.; Skulan, A. J.; Yang, Y. S.; Zhou, J. *Chem. Rev.* **2000**, *100*, 235. (b) Decker, A.; Solomon, E. I. *Angew. Chem., Int. Ed.* **2005**, *44*, 2252. (c) Neese, F. *J. Inorg. Biochem.* **2006**, *100*, 716. (d) Ghosh, A.; Tangen, E.; Ryeng, H.; Taylor, P. R. *Eur. J. Inorg. Chem.* **2004**, *23*, 4555. (e) Kumar, D.; Hirao, H.; Que, L., Jr.; Shaik, S. *J. Am. Chem. Soc.* **2005**, *127*, 8026. (f) Kamachi, T.; Kouno, T.; Nam, W.; Yoshizawa, K. *J. Inorg. Biochem.* **2006**, *100*, 751. (g) de Visser, S. P. *Angew. Chem., Int. Ed.* **2006**, *45*, 1790. (h) Pestovsky, O.; Stoian, S.; Bominaar, E. L.; Shan, X.; Münck, E.; Que, L., Jr.; Bakac, A. *Angew. Chem., Int. Ed.* **2005**, *117*, 7031. (i) Anastasi, A. E.; Comba, P.; McGrady, J.; Lienke, A.; Rohwer, H. *Inorg. Chem.* **2007**, *46*, 6420. (j) Dey, A.; Ghosh, A. *J. Am. Chem. Soc.* **2002**, *124*, 3206. (k) Groves, J. T.; Gross, Z.; Stern, M. K. *Inorg. Chem.* **1994**, *33*, 5065. (l) van den Berg, T. A.; de Boer, J. W.; Browne, W. R.; Roelfes, G.; Feringa, B. L. *Chem. Commun.* **2004**, 2550. (m) Kozlowski, P. M.; Kuta, J.; Ohta, T.; Kitagawa, T. *J. Inorg. Biochem.* **2006**, *100*, 744. (n) Terner, J.; Palaniappan, V.; Gold, A.; Weiss, R.; Fitzgerald, M. M.; Sullivan, A. M.; Hosten, C. M. *J. Inorg. Biochem.* **2006**, *100*, 480. (o) Grapperhaus, C. A.; Mienert, B.; Bill, E.; Weyhermüller, T.; Wieghardt, K. *Inorg. Chem.* **2000**, *39*, 5306.

(15) (a) Decker, A.; Rohde, J.-U.; Que, L., Jr.; Solomon, E. I. *J. Am. Chem. Soc.* **2004**, *126*, 5378. (b) Jensen, M. P.; Lange, S. M.; Mehn, M. P.; Que, E. L.; Que, L., Jr. *J. Am. Chem. Soc.* **2003**, *125*, 2113.

(16) Aquino, F.; Rodriguez, J. H. *J. Chem. Phys.* **2005**, *123*, 204902.

(17) Cho, J.; Jeon, S.; Wilson, S. A.; Liu, L. V.; Kang, E. A.; Braymer, J. J.; Lim, M. H.; Hedman, B.; Hodgson, K. O.; Valentine, J. S.; Solomon, E. I.; Nam, W. *Nature* **2011**, *748*, 502.

(18) Prat, I.; Mathieson, J. S.; Güell, M.; Ribas, X.; Luis, J. M.; Cronin, L.; Costas, M. *Nat. Chem.* **2011**, *3*, 788.

(19) (a) de Oliveira, F. T.; Chanda, A.; Banerjee, D.; Shan, X.; Mondal, S.; Que, L., Jr.; Bominaar, E. L.; Münck, E.; Collins, T. J. *Science* **2007**, *315*, 835. (b) Lyakin, O. Y.; Bryliakov, K. P.; Britovsek, G. J. P.; Talsi, E. P. *J. Am. Chem. Soc.* **2009**, *131*, 10798.

(20) McDonald, A. R.; Que, L., Jr. *Nat. Chem* **2011**, *3*, 761.

(21) Van Heuvelena, K. M.; Fiedlera, A. T.; Shana, X.; De Hontc, R. F.; Meierc, K. K.; Bominaar, E. L.; Münck, E.; Que, L., Jr. *Proc. Natl. Acad. Sci. U.S.A.* **2012**, *109*, 11933.
(22) Taktak, S.; Flook, M.; Foxman, B. M.; Que, L., Jr.; Rybak-Akimova, E. V. *Chem. Commun.* **2005**, 5301.
(23) (a) Ho, R. Y. N.; Roelfes, G.; Feringa, B. L.; Que, L., Jr. *J. Am. Chem. Soc.* **1999**, *121*, 264. (b) Mairata i Payeras, A.; Ho, R. Y. N.; Fujita, M.; Que, L., Jr. *Chem.—Eur. J.* **2004**, *10*, 4944.
(24) Thibon, A.; Jollet, V. R.; Ribal, C.; Sénéchal-David, K.; Billon, L.; Sorokin, A. B.; Banse, F. *Chem.—Eur. J.* **2012**, *18*, 2715.
(25) (a) Foster, T. L.; Caradonna, J. P. *J. Am. Chem. Soc.* **2003**, *125*, 3678. (b) Que, L., Jr.; Ho, R. Y. N. *Chem. Rev.* **1996**, *96*, 2607. (c) Donald, W. A.; McKenzie, C. J.; O'Hair, R. A. J. *Angew. Chem., Int. Ed.* **2011**, *50*, 8379. (d) Seo, M. S.; Kim, N. H.; Cho, K.-B.; So, J. E.; Park, S. K.; Clemancey, M.; Garcia-Serres, R.; Latour, J.-M.; Shaik, S.; Nam, W. *Chem. Sci.* **2011**, *2*, 1039.
(26) Mas-Ballesté, R.; Que, L., Jr. *J. Am. Chem. Soc.* **2007**, *129*, 15964.
(27) Park, M. J.; Lee, J.; Suh, Y.; Kim, J.; Nam, W. *J. Am. Chem. Soc.* **2006**, *128*, 2630.
(28) Chow, M. S.; Liu, L. V.; Solomon, E. I. *Proc. Natl. Acad. Sci. U.S.A.* **2008**, *105*, 13241.
(29) Hirao, H.; Li, F.; Que, L., Jr.; Morokuma, K. *Inorg. Chem.* **2011**, *50*, 6637.
(30) (a) Buijs, W.; Comba, P.; Corneli, D.; Pritzkow, H. *J. Organomet. Chem.* **2002**, *641*, 71. (b) Reinaud, O.; Capdevielle, P.; Maumy, M. *J. Chem. Soc., Chem. Commun.* **1990**, 556. (c) Comba, P.; Knoppe, S.; Martin, B.; Rajaraman, G.; Rolli, C.; Shapiro, B.; Stork, T. *Chem.—Eur. J.* **2008**, *14*, 344.
(31) Frisch, M. J.; et al. *Gaussian 09*, revision 02; Gaussian, Inc.: Wallingford, CT, 2009
(32) (a) Grimme, S.; Antony, J.; Ehrlich, S.; Krieg, H. *J. Chem. Phys.* **2010**, *132*, 154104. (b) Grimme, S. *J. Comput. Chem.* **2006**, *27*, 1787.
(33) (a) Olsson, E.; Mertinez, A.; Teigen, K.; Jensen, V. R. *Eur. J. Inorg. Chem.* **2011**, 2720. (b) Olsson, E.; Mertinez, A.; Teigen, K.; Jensen, V. R. *Eur. J. Inorg. Chem.* **2011**, *17*, 3746.
(34) (a) Isabella, H.-K.; Mück-Lichtenfeld, C.; Grimme, S. *Croat. Chem. Acta* **2009**, *82*, 115. (b) Neese, F.; Zaleski, J. M.; Zaleski, K. L.; Solomon, E. I. *J. Am. Chem. Soc.* **2000**, *122*, 11703. (c) Greco, C.; Bruschi, M.; Fantucci, P.; Ryde, U.; De Gioio, L. *J. Am. Chem. Soc.* **2011**, *133*, 18742. (d) Dey, A.; Jiang, Y.; de Montellano, P. O.; Hodgson, K. O.; Hedman, B.; Solmon, E. I. *J. Am. Chem. Soc.* **2009**, *131*, 7869. (e) Hirao, H.; Kumar, D.; Que, L., Jr.; Shaik, S. *J. Am. Chem. Soc.* **2006**, *128*, 8590. (f) Hirao, H.; Kumar, D.; Thiel, W.; Shaik, S. *J. Am. Chem. Soc.* **2005**, *127*, 13007. (g) Bathelt, C. M.; Zurek, J.; Mulholland, A. J.; Harvey, J. N. *J. Am. Chem. Soc.* **2005**, *127*, 12900. (h) Bassan, A.; Blomberg, M. R. A.; Siegbahn, P. E. M.; Que, L., Jr. *Angew. Chem., Int. Ed.* **2005**, *44*, 2939. (i) Siegbahn, P. E. M.; Borowski, T. *Acc. Chem. Res.* **2006**, *39*, 729. (j) Siegbahn, P. E. M. *J. Biol. Inorg. Chem.* **2006**, *11*, 695. (k) Ghosh, A. *J. Biol. Inorg. Chem.* **2006**, *11*, 671. (l) Neese, F. *J. Biol. Inorg. Chem.* **2006**, *11*, 702. (m) Noodleman, L.; Han, W.-G. *J. Biol. Inorg. Chem.* **2006**, *11*, 674. (n) Ghosh, A. *J. Biol. Inorg. Chem.* **2006**, *11*, 712.
(35) Chai, J.-D.; Head-Gordon, M. *Phys. Chem. Chem. Phys.* **2008**, *10*, 6615.
(36) Zhao, Y.; Truhlar, D. G. *Theor. Chem. Acc.* **2008**, *120*, 215.
(37) Staroverov, V. N.; Scuseria, G. E.; Tao, J.; Perdew, J. P. *J. Chem. Phys.* **2003**, *119*, 12129.
(38) Handy, N. C.; Cohen, A. J. *Mol. Phys.* **2001**, *99*, 401.
(39) Møller, C.; Plesset, M. S. *Phys. Rev.* **1934**, *46*, 618.
(40) (a) Li, F.; Meier, K. K.; Cranswick, M. A.; Chakrabarti, M.; Van Heuvelen, K. M.; Münck, E.; Que, L., Jr. *J. Am. Chem. Soc.* **2011**, *133*, 7256. (b) Fujii, T.; Ozawa, T.; Funahashi, Y.; Jitsukawa, K.; Masudab, H. *Adv. Mater. Res.* **2006**, *11–12*, 331.
(41) (a) Lim, M. H.; Rohde, J.-U.; Stubna, A.; Bukowski, M. R.; Costas, M.; Ho, R. Y. N.; Münck, E.; Nam, W.; Que, L., Jr. *Proc. Natl. Acad. Sci. U.S.A.* **2003**, *100*, 3665. (b) Rohde, J.-U.; Stubna, A.; Bominaar, E. L.; Münck, E.; Nam, W.; Que, L., Jr. *Inorg. Chem.* **2006**, *45*, 6435. (c) Bukowski, M. R.; Koehntop, K. D.; Stubna, A.; Bominaar, E. L.; Halfen, J. A.; Münck, E.; Nam, W.; Que, L., Jr. *Science* **2005**, *310*, 1000.
(42) Chen, H.; Lai, W.; Shaik, S. *J. Phys. Chem. Lett.* **2010**, *1*, 1533.
(43) (a) Boguslawski, K.; Jacob, C. R.; Reiher, M. *J. Chem. Theory Comput.* **2011**, *7*, 2740. (b) Kepp, K. P. *Coord. Chem. Rev.* **2013**, *257*, 196. (c) Ye, S.; Neese, F. *Inorg. Chem.* **2010**, *49*, 772.
(44) (a) Dunning, T. H., Jr.; Hay, P. J. In *Modern Theoretical Chemistry*; Schaefer, H. F., III, Ed.; Plenum: New York, 1976; Vol. *3*, p 1. (b) Hay, P. J.; Wadt, W. R. *J. Chem. Phys.* **1985**, *82*, 270. (c) Wadt, W. R.; Hay, P. J. *J. Chem. Phys.* **1985**, *82*, 284. (d) Hay, P. J.; Wadt, W. R. *J. Chem. Phys.* **1985**, *82*, 299.
(45) Ditchfield, R.; Hehre, W. J.; Pople, J. A. *J. Chem. Phys.* **1971**, *54*, 724.
(46) (a) Schäfer, A.; Horn, H.; Ahlrichs, R. *J. Chem. Phys.* **1992**, *97*, 2571. (b) Schäfer, C.; Huber, C.; Ahlrichs, R. *J. Chem. Phys.* **1994**, *100*, 5829.
(47) (a) Fluckiger, P.; Luthi, H. P.; Portmann, S.; Weber, J. *Molekel 4.3*; Swiss Center for Scientific Computing: Manno, Switzerland, 2000. (b) Portmann, S.; Lüthi, H. P. *Chimia* **2000**, *54*, 766.
(48) (a) Noodleman, L. *J. Chem. Phys.* **1981**, *74*, 5737. (b) Harvey, J. N.; Aschi, M.; Schwarz, H.; Koch, W. *Theor. Chem. Acc.* **1998**, *99*, 95.
(49) (a) Bassan, A.; Blomberg, M. R. A.; Siegbahn, P. E. M.; Que, L., Jr. *J. Am. Chem. Soc.* **2002**, *124*, 11056. (b) Bassan, A.; Blomberg, M. R. A.; Siegbahn, P. E. M.; Que, L., Jr. *Chem.—Eur. J.* **2005**, *11*, 692. (c) Ghosh, A.; Almlöf, J.; Que, L., Jr. *Angew. Chem., Int. Ed. Engl.* **1996**, *35*, 770. (d) Lehnert, N.; Neese, F.; Ho, R. Y.; Que, L., Jr.; Solomon, E. I. *J. Am. Chem. Soc.* **2002**, *124*, 10810. (e) Lehnert, N.; Ho, R. Y.; Que, L., Jr.; Solomon, E. I. *J. Am. Chem. Soc.* **2002**, *123*, 8271. (f) Chen, H.; Lai, W. Z.; Yao, J. N.; Shaik, S. *J. Chem. Theory. Comput.* **2011**, *7*, 3049.
(50) Derat, E.; Kumar, D.; Hirao, H.; Shaik, S. *J. Am. Chem. Soc.* **2006**, *128*, 473.
(51) (a) Bassan, A.; Blomberg, M. R. A.; Siegbahn, P. E. M.; Que, L., Jr. *Chem.—Eur. J.* **2005**, *11*, 692. (b) Bassan, A.; Blomberg, M. R. A.; Siegbahn, P. E. M. *Chem.—Eur. J.* **2003**, *9*, 4055.
(52) (a) Weiss, R.; Bulach, V.; Gold, A.; Terner, J.; Trautwein, A. X. *J. Biol. Inorg. Chem.* **2001**, *6*, 831. (b) Comba, P.; Maurer, M.; Vadivelu, P. *J. Phys. Chem. A* **2008**, *112*, 13028. (c) Quinonero, D.; Morokuma, K.; Musaev, D. G. *J. Am. Chem. Soc.* **2005**, *127*, 6548. (d) Chakrabarty, S.; Austin, R. N.; Deng, D.; Groves, J. T.; Lipscomb, J. D. *J. Am. Chem. Soc.* **2007**, *129*, 3514.
(53) (a) Newcomb, M.; Zhang, R.; Chandrasena, R. E. P.; Halgrimson, J. A.; Horner, J. H.; Makris, T. M.; Sligar, S. G. *J. Am. Chem. Soc.* **2006**, *128*, 4580. (b) Noack, H.; Siegbahn, P. E. M. *J. Biol. Inorg. Chem.* **2007**, *12*, 1151.
(54) This estimate is obtained by performing single-point calculations with B3LYP-D3 on B3LYP-optimized geometry.
(55) (a) Cho, K.-B.; Wu, X.; Lee, Y.-M.; Kwon, Y. H.; Shaik, S.; Nam, W. *J. Am. Chem. Soc.* **2012**, *134*, 20222. (b) Wilson, S. A.; Chen, J.; Hong, S.; Lee, Y.-M.; Clémancey, M.; Garcia-Serres, R.; Nomura, T.; Ogura, T.; Latour, J.-M.; Hedman, B.; Hodgson, K. O.; Nam, W.; Solomon, E. I. *J. Am. Chem. Soc.* **2012**, *134*, 11791. (c) Johansson, A. J.; Blomberg, M. R. A.; Siegbahn, E. M. *J. Phys. Chem. C* **2007**, *111*, 12397. (d) Geng, C.; Ye, S.; Neese, F. *Angew. Chem., Int. Ed.* **2010**, *49*, 5717. (e) Reiher, M.; Hess, B. A. *Chem.—Eur. J.* **2002**, *8*, 5332. (f) Bassan, A.; Blomberg, M. R. A.; Siegbahn, P. E. M. *J. Biol. Inorg. Chem.* **2004**, *9*, 439.
(56) (a) Schröder, D.; Shaik, S.; Schwarz, H. *Acc. Chem. Res.* **2000**, *33*, 139. (b) Goossen, L. J.; Koley, D.; Hermann, H. L.; Thiel, W. *J. Am. Chem. Soc.* **2005**, *127*, 11102.
(57) Ye, S.; Neese, F. *Proc. Natl. Acad. Sci. U.S.A.* **2011**, *108*, 1228.
(58) Solomon, E. I.; Decker, A.; Lehnert, N. *Proc. Nat. Acad. Sci. U.S.A.* **2003**, *100*, 3589.
(59) (a) Cano, J.; Ruiz, E.; Alvarez, S.; Verdaguer, M. *Comments Inorg. Chem.* **1998**, *20*, 27. (b) Ruiz, E.; Alvarez, S.; Rodriguez-Fortea, A.; Alemany, P.; Pouillon, Y.; Massobrio, C. *Magnetism: Molecules to Materials*; Miller, J. S., Drillon, M., Eds.; Wiley-VCH: Weinheim, 2001; Vol. *II*, p 227.
(60) (a) Quesne, M. G.; de Visser, S. P. *J. Biol. Inorg. Chem.* **2012**, *17*, 814. (b) Jensen, M. P.; Costas, M.; Ho, R. Y. N.; Kaizer, J.; Mairata i

Payerras, A.; Münck, E.; Que, L., Jr.; Rohde, J.-U.; Stubna, A. *J. Am. Chem. Soc.* **2005**, *127*, 10512.
(61) (a) Ogliaro, F.; Harris, N.; Cohen, S.; Filatov, M.; de Visser, S. P.; Shaik, S. *J. Am. Chem. Soc.* **2000**, *122*, 8977. (b) Schöneboom, J. C.; Cohen, S.; Lin, H.; Shaik, S.; Thiel, W. *J. Am. Chem. Soc.* **2004**, *126*, 4017. (c) de Visser, S. P.; Shaik, S.; Sharma, P. K.; Kumar, D.; Thiel, W. *J. Am. Chem. Soc.* **2003**, *125*, 15779. (d) Kumar, D.; de Visser, S. P.; Shaik, S. *J. Am. Chem. Soc.* **2004**, *126*, 5072.
(62) Janardanan, D.; Wang, Y.; Schyman, P.; Que, L., Jr.; Shaik, S. *Angew. Chem., Int. Ed.* **2010**, *49*, 3342.
(63) Shaik, S.; Chen, H.; Janardanan, D. *Nat. Chem.* **2011**, *3*, 19.